AD-A136 891 STRENGTH AND THERMAL SHOCK RESISTANCE OF SIC-BN COMPOSITES(U) AIR FORC INST OF TECH WRIGHT-PATTERSON AFB OH SCHOOL OF ENGINEERING P G VALENTINE DEC 83 1/1

UNCLASSIFIED AFIT/GAE/AA/83D-27 F/G 11/2 NL

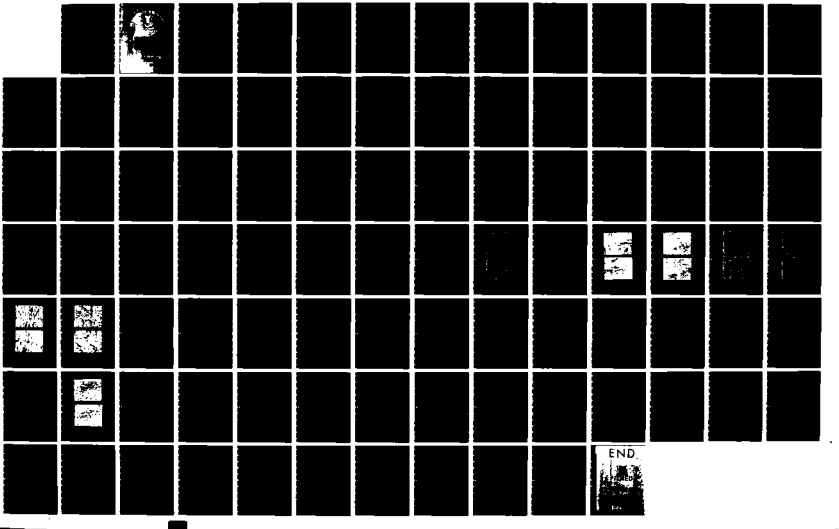

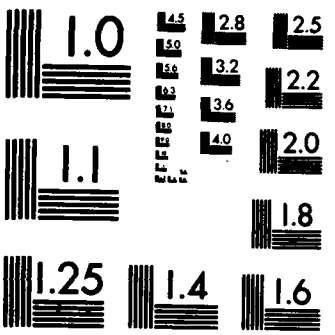

STRENGTH AND THERMAL SHOCK RESISTANCE OF SiC-BN COMPOSITES

THESIS

Peter G. Valentine
First Lieutenant, USAF

AFIT/GAE/AA/83D-27

AFIT/GAE/AA/83D-25

STRENGTH AND THERMAL SHOCK RESISTANCE OF SiC-BN COMPOSITES

THESIS

Peter G. Valentine
First Lieutenant, USAF

AFIT/GAE/AA/83D-27

AFIT/GAE/AA/83D-25

STRENGTH AND THERMAL SHOCK RESISTANCE OF SiC-BN COMPOSITES

THESIS

Presented to the Faculty of the School of Engineering

of the Air Force Institute of Technology

Air University

In Partial Fulfillment of the

Requirements for the Degree of

Master of Science in Aeronautical Engineering

Peter G. Valentine, M.S.

First Lieutenant, USAF

December 1983

Acknowledgements

I wish to acknowledge the encouragement and assistance that everyone at Wright-Patterson Air Force Base has given me in completing this thesis. The Processing and High Temperature Materials Branch (MLLM), which is part of AFWAL/MLL at Wright-Patterson AFB, supported this work.

Several members of the AFIT faculty and the AFWAL/ML laboratories need to be acknowledged. I wish to thank the members of my thesis committee, Dr. A.N. Palazotto, LTC G.W. Watt, and MAJ G.K. Haritos, and several members of the AFWAL laboratories, J. Barlowe, G. Cornish, J. Henry, E. Hermes, W. Kerr, K. Mazdiyasni, J. Muntz, R. Ruh, and J. Workman. Their efforts, and those of everyone else at Wright-Patterson AFB, are greatly appreciated. I would especially like to thank Dr. Ruh and Dr. Palazotto for everything that they have done in helping me conduct and document this study.

I would like to thank D.P.H. Hasselman (Virginia Polytechnic Institute and State University, Blacksburg, Virginia) and D.C. Larsen (Illinois Institute of Technology Research Institute, Chicago, Illinois) for their assistance in conducting this study. I would also like to thank M.J. Gerhardt for her encouragement and assistance.

Peter G. Valentine

Table of Contents

List of Figures

List of Tables

Abstract

The strength and thermal shock behavior of hot-pressed silicon-carbide/boron-nitride (SiC-BN) particulate composites were investigated for compositions of 0, 8.8, 17.9, and 27.2 volume percent BN. Using bend strength, Young's modulus of elasticity, density, and coefficient of thermal expansion data, the thermal stress resistance parameters R, R", and R''' were calculated and, for the R parameters, compared with experimental values for critical quench temperatures (ΔT).

Composite microstructures were characterized by x-ray diffraction (XRD) analysis, density determinations, light microscopy (LM), and scanning electron microscopy (SEM). Specimen microstructures were shown to consist of a SiC matrix with BN plates oriented perpendicular to the direction in which the load was applied during hot-pressing. Young's moduli were determined to be highly dependent on the BN content, with values decreasing with increasing vol. % BN.

In general, over the composition range of 0 to 27.2 vol. % BN and the temperature range of 22° to 1500°C, changes in the BN content seemed to have a minimal effect on the strength of the SiC-BN composites. However, a fine-grained 0 vol. % BN-SiC specimen showed a dramatic increase in strength with increasing temperature, probably caused by relaxation of residual stresses. No distinct pattern was evident for change in strength as a function of BN content at constant temperature, probably due to the small number of specimens considered, although the strength is expected to decrease with increasing BN content.

Water-quench thermal shock tests showed that increasing the BN content increased the maximum change in temperature that the composites

could survive. Increasing the BN content was observed to increase the resistance of the composites to crack initiation (increase R and R"), while decreasing the resistance to crack propagation damage (decrease R'''). Grain size and anisotropy effects were also considered, with both influencing the bend strength and thermal stress resistance parameters to some extent.

STRENGTH AND THERMAL SHOCK RESISTANCE OF SiC-BN COMPOSITES

I. Introduction

Silicon-Carbide/Boron-Nitride Composites

Studies carried out on silicon-carbide/boron-nitride (SiC-BN) composites have dealt primarily with aerospace applications. SiC-BN composites have been considered for use in gas turbine jet engines and in other structural high-temperature applications. Hillig (1) used a BN/Si/SiC layer on ceramic shrouds as a blade-tip seal and in a stacked ring combustor as a compliant layer at ceramic/ceramic and ceramic/metal interfaces. Compliant BN/Si/SiC layers were initially developed by Mehan et al. (2) for their impact absorption capabilities when applied to Si-SiC substrates. These studies and an investigation by Bentsen et al. (3), into the thermal diffusivity anisotropy of SiC-BN composites, dealt with particulate composites.

Investigations by Mehan et al. (2) into structural applications of silicon carbide ceramic materials determined that BN/Si/SiC compliant materials are effective in relieving localized high stresses and providing impact resistance. Such compliant materials, which crush at a threshold compressive stress and redistribute the load over a more extensive bearing surface, have been found to be capable of preventing impact damage either by high velocity projectiles or vibration-induced chattering at contact points. By varying the BN content a balance could be obtained between impact and erosion resistance for specific applications. The compliant layers also provided some degree of thermal

insulation for the base materials.

Hasselman's Theory on the Resistance of High-E, Low-E Brittle Composites to Failure by Thermal Shock

Hasselman's theory (4) states that the inclusion of a dispersed phase with low Young's modulus will significantly improve the generally low thermal stress resistance of brittle materials (with high Young's modulus) for high-temperature applications. In designing such composites the parameters that should be considered are as follows: 1) the elastic or Young's modulus (E), 2) the fracture stress (σ), 3) the shape and distribution of the low-E phase, 4) the amount of porosity, 5) the dispersed phase particle size, 6) the thermal diffusivity (a), 7) the phases of the component materials, 8) the coefficient of thermal expansion (α), and 9) Poisson's ratio (ν). For high/low modulus composites, parameters 1) through 5) have the greatest influence on thermal stress resistance, while parameters 8) and 9) have only a minimal effect.

For high-temperature applications, brittle materials are highly susceptible to catastrophic failure under conditions of severe thermal shock. Often for high-temperature structures or components, thermal stresses of such severity will occur that failure of even the best material available cannot be avoided. Thus, materials should be selected which will retain their geometrical and physical characteristics to the extent that the material can still function in a satisfactory manner even after some crack propagation has occurred. By developing materials with the proper combination of properties, the magnitude of the thermal stress can be reduced or the effect of thermal stress failure on subsequent material performance can be minimized. The role these physical

properties play in determining the thermal stress failure of brittle materials has been characterized by thermal stress resistance parameters (discussed later). Materials with high values of these parameters exhibit a high resistance to the initiation of themal stress fracture and show less of a tendency towards catastrophic or unstable crack propagation. Unfortunately, having a high resistance to the initiation of thermal stress failure requires a high value of tensile strength and a low value of Young's modulus of elasticity, while minimizing the extent of crack propagation requires a low value of tensile strength with a high value of Young's modulus. Thus, materials with high values of the thermal stress resistance parameters characterizing resistance to the initiation of thermal stress fracture have low values of the parameters characterizing resistance to crack propagation, and vice versa.

Hasselman states that a solution to this dilemma is offered by continuous matrix-dispersed phase composites. Examples of such composites are as follows: 1) carbides of silicon, zirconium (5), or boron containing dispersed phases of graphite, 2) hyper-eutectic carbides of hafnium or zirconium with graphite precipitates (6), 3) glass with a mica dispersed-phase, and 4) aluminum oxide with dispersions of boron nitride. Higher levels of heat flux are required to initiate thermal stress fracture in these composites than in the matrix materials without their dispersed phases. Also, the presence of the dispersions reduces the likelihood of the highly catastrophic failure mode of the pure matrix phase. For these composites the dispersed phase has a Young's modulus of elasticity much less than that of the corresponding continuous matrix phase. Thus, such materials are referred to as high-E, low-E

composites since the mismatch in elastic properties is responsible for the improvement in thermal fracture behavior.

The presence of the low-E phase has a significant effect on most of the properties of the matrix phase, although the coefficient of thermal expansion and Poisson's ratio are effected little if any at even high volume fractions. Inclusion of the low-E phase in the matrix alters the thermal conductivity, but changes in the thermal conductivity of the matrix do not appear to be responsible for the improvement in thermal fracture behavior. Both the Young's modulus and the tensile fracture stress decrease significantly when a low-E phase is added to a high-E matrix, while the fracture energy, which is beneficial for rapid crack arrest, increases due to the low-E phase promoting non-planar crack propagation. Therefore, improvement in the thermal fracture behavior, when a low-E phase is added to a high-E material, can be attributed primarily to the combined changes in the elastic behavior, the fracture stress, and the fracture energy.

The size, shape, distribution, and type of second phase particles have important effects on the thermal fracture behavior of the composite materials. From the mechanical point of view the low-E dispersed phase has approximately the same effect on the matrix as does porosity. The low-E dispersed phase is much preferred, though, because it permits control over the shape of the inclusion and causes a much smaller decrease in thermal conductivity than does porosity, thus aiding in improving the thermal stress resistance of the composite material. According to Hasselman et al. (4) for the high-E, low-E concept to be effective, the low-E phase must be in the form of a dispersed phase because a

continuous low-E phase would allow failure initiation to occur in the low-E phase. Thus, a continuous low-E phase would probably decrease the thermal stress resistance since materials with a low Young's modulus usually have low strength. The high-E, low-E theory was developed for spherical particles, although it can also be applied to elliptically shaped second phase particles such as those that occur during hot-pressing. Hasselman et al. (4) believed, though, that such elliptically-shaped phases would cause anisotropy of the continuum properties of the composites.

In summary, the thermal stress resistance of brittle materials with high values of Young's modulus can be improved significantly by the addition of a dispersed phase with much lower Young's modulus. These dispersions not only improve the strain-at-fracture, which improves the resistance to the initiation of thermal stress failure, but also reduce the elastic energy at fracture and improve the fracture energy to inhibit extensive crack propagation after failure (4).

Objectives and Reasons for the Present Study

The purpose of this investigation was to determine the mechanical behavior (i.e. strength and thermal shock resistance) of silicon-carbide /boron-nitride composites and to test D.P.H. Hasselman's theory for high/low modulus composites. The primary objectives of this study were, therefore, as follows: 1) to experimentally determine the material properties and thermal stress resistance parameters for SiC-BN composites, 2) to ascertain if the thermal stress resistance of SiC is significantly improved as predicted by Hasselman's theory, and 3) to determine how the strength of SiC-BN composites varies with changes in BN-content and

temperature. A study that dealt with the Si_3N_4-BN system (7) determined that Hasselman's theory held for that system, but Si_3N_4 is significantly different from SiC (for example: the Young's moduli are 0.310×10^6 MPa and 0.448×10^6 MPa, respectively). Thus, it was not known if the theory could be applied to the SiC-BN system.

Certain ceramics, such as silicon carbide, can exhibit high strength and oxidation resistance at temperatures 400-600°C greater than the maximum operating temperatures of nickel and cobalt superalloys (8) in gas turbine jet engines. Thus, by increasing the operating temperatures of gas turbines through the use of ceramic stator vanes, rotor blades, etc., the thermal efficiency and specific power output can be increased while the fuel consumption is lowered. Ceramics considered for such applications have densities of 2.5-3.2 gm/cm^3 while those of superalloys are approximately 8 gm/cm^3. Thus, the weight of an engine and the stresses in parts such as rotor blades could be reduced through the use of ceramics; the centrifugal stress developed in rotor blades is directly proportional to their density. Also, it can be much cheaper to obtain the raw materials and fabricate ceramic parts than it is to produce superalloy components. Ceramic materials also have generally better high-temperature corrosion resistance than do superalloys. Therefore, there are numerous reasons why ceramics are being considered for use in gas turbine jet engines.

The primary problems associated with the use of SiC in jet engines are that silicon carbide is extremely brittle and has little thermal shock resistance. Thus, the present study was conducted to see if additions of BN could improve the thermal shock resistance of SiC as predicted by Hasselman's theory.

II. Theoretical Considerations

Thermal Stresses and Thermal Shock Failure in Ceramics

Stresses resulting from temperature gradients are defined as thermal stresses (9). Each time the temperature of an experimental sample or structural body is changed thermal stresses occur because of the resulting temperature gradients. The importance of these stresses depends on their magnitude. The origin of thermal stresses is the difference in thermal expansion of various parts of a body under conditions such that free expansion of each small unit of volume cannot take place (11). One way in which thermal stresses can be generated is by thermal shock. According to Kingery (9), thermal shock corresponds to a sudden temperature change, as opposed to steady-state stresses, which may also be substantial. Burgreen (10) has defined thermal shock as the generation of non-inertial thermal stresses by rapid changes in the temperature distribution within a body. Thermal shock is often produced by the sudden application of a hot or cold fluid to the surface of a structure.

The susceptibility of ceramic materials to thermal stresses and thermal shock failure is a primary factor in limiting their usefulness (12). During transient heating and cooling conditions, the low thermal conductivity of many ceramic materials causes termperature gradients to occur within the bodies of the materials. The stresses that are developed within the body are proportional to the temperature difference between adjacent volume elements and arise because of constraint of these volume elements on one another.

Changing the temperature of a body from an initial termperature,

T_0, to a new uniform temperature, T_1, will cause no stresses provided the body is homogeneous, isotropic, and unrestrained or free to expand. In this situation, the expansion of each volume element is $\alpha(T_1-T_0)$, where α is the coefficient of thermal expansion, and the shape of the body is unchanged. On the other hand, if the body is not homogeneous and isotropic, such as a polycrystalline material with anisotropic crystals, a multiphase material, etc., stresses will result from the difference in expansion between crystals or phases. In extreme cases, serious weakening or fracture may occur. Stresses may also result if a structure is completely constrained from expanding or contracting through the use of restraining forces. Stresses such as these, while not due to a temperature gradient and therefore not classified as thermal stresses as defined by Kingery (9), will be additive with any thermal stresses developed and must be considered in many practical applications of thermal stress.

The existence of a temperature gradient does not necessarily mean that thermal stresses will occur, although in general such stresses will occur. An infinite slab, made from a homogeneous and isotropic material, with a linear temperature gradient would be a case in which the body can expand or contract without incompatible strains and no stresses would result. Usually, though, temperature is not a linear function of dimension, and the free expansion of volume elements would lead to separation of the elements so that the body would no longer be continuous. Since each element is constrained by the rest of the body, thermal stresses will result. Thus, it can be seen that the temperature distribution must be known if thermal stresses are to be calculated.

In the steady state, the temperature distribution is determined by the rate of heat flow, the specimen shape, and the thermal conductivity. In the unsteady or transient state, the change in the temperature at a particular point with respect to time will depend on the thermal conductivity and the heat capacity per unit volume. In any situation, determining the stresses in a structure requires knowledge of the heat transfer conditions and the temperature distribution, along with the elastic and thermal material constants for the structure.

Thermal Shock Resistance

Substantial stresses develop when ceramic materials are subjected to rapid changes in temperature. Thermal endurance, thermal stress resistance, or thermal shock resistance is the resistance to fracture or weakening under such conditions. Different materials are effected differently by thermal stresses because, in addition to the stress level, the stress distribution in the body, and the stress duration, material characteristics such as ductility, homogeneity, porosity, pre-existing flaws, etc., are important (13). Consequently, defining a single thermal-stress-resistance factor for use in all situations is impossible.

Two approaches can be taken to the problem of thermal shock; consideration of the nucleation of cracks or consideration of the propagation of pre-existing cracks. When considering the conditions which govern the nucleation of fracture, the assumption is made that failure occurs when the thermal stress reaches the fracture stress. The maximum quench temperatures that can be withstood using this failure criterion for different materials and different conditions of heat transfer are shown in Fig. 1. In general, as the rate of heat transfer increases,

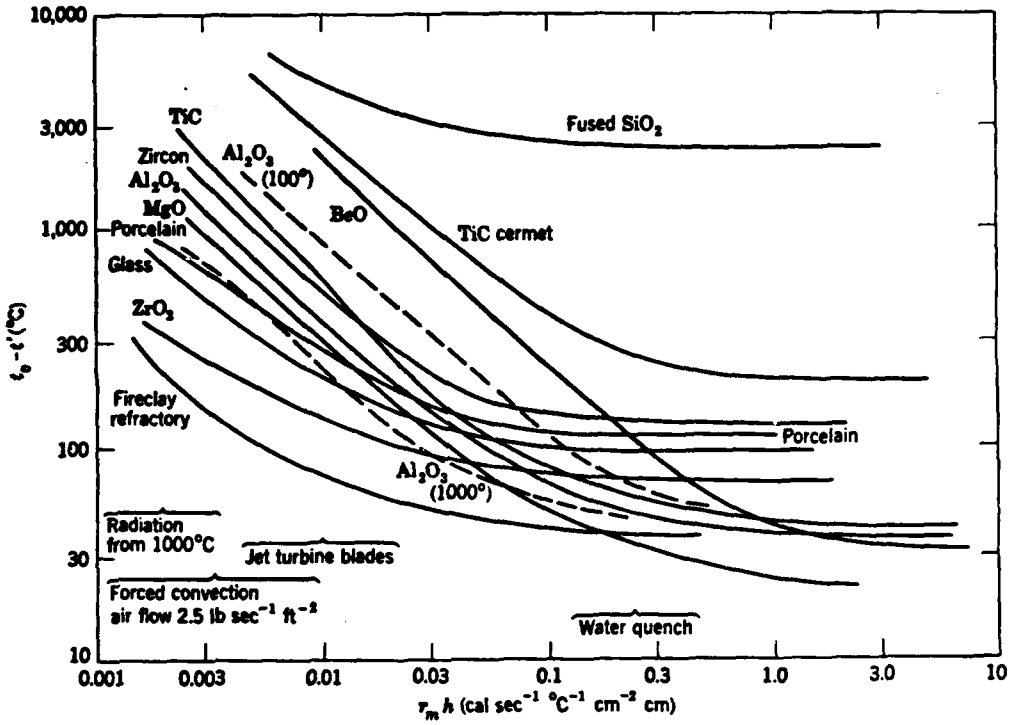

Symbols: r_m - parameter that depends on geometry of material, called the half thickness

h - surface heat-transfer coefficient

t_0 - initial temperature

t' - new temperature

Figure 1. Variation in Quench Temperature Causing Fracture for Different Materials under Different Conditions of Heat Transfer (9, 13).

Failure is assumed to occur when the thermal stress reaches the fracture stress. Curves are calculated from material properties at 400°C. Dashed curves for Al_2O_3 are calculated from material properties at 100° and 1000°C, as an indication of temperature effects.

the degree of thermal shock (the change in temperature that a material can withstand) decreases. The curves for a number of materials cross, indicating that as the rate of heat transfer changes, certain materials

will be effected to a greater extent by thermal stresses than others. Thus, even for a given criterion of failure, materials cannot be listed in a single order of thermal stress resistance. Since different types of heat transfer may occur, such as steady-state heat flow out through the walls of a hollow cylinder, constant rate of heating from the surface, and cooling by radiation from an elevated temperature, different material properties and constants may need to be evaluated in order to determine a relative ranking of the thermal stress resistance of the materials under consideration. According to Kingery (14), the properties which affect thermal stress resistance are elastic modulus, strength, coefficient of expansion, Poisson's ratio, and, in some cases, thermal conductivity, diffusivity, or emissivity.

Treating the conditions which govern the propagation of cracks (described previously as the second thermal shock approach), Hasselman (15,16) noted that the driving force for crack propagation is provided by the elastic energy released at the moment of fracture. Crack propagation under thermal stress conditions generally occurs in the absence of external forces. The critical termperature difference ΔT_c required for crack instability has been derived from an expression for the total energy per unit volume W_T, which is the sum of the elastic energy plus fracture energy of the cracks, using the fact that cracks are unstable between those limits for which (15)

$$\frac{dW_T}{dL} = 0 \qquad (1)$$

The critical temperature difference is given as

$$\Delta T_c = \left[\frac{\pi \gamma_{eff}(1-2\nu)^2}{2E_o\alpha^2(1-\nu^2)}\right]^{\frac{1}{2}} \left[1+\frac{16(1-\nu^2)NL^3}{9(1-2\nu)}\right] L^{-\frac{1}{2}} \qquad (2)$$

where crack propagation is assumed to occur by the simultaneous propagation of N cracks per unit volume. E_o is the Young's modulus of the crack free material, γ_{eff} is the fracture surface work, ν is Poisson's ratio, α is the coefficient of thermal expansion, and L is the crack length. This equation (Eq. 2) is represented by the solid lines in Fig. 2. Note that, in general, the region of crack instability is bounded by two values of crack length.

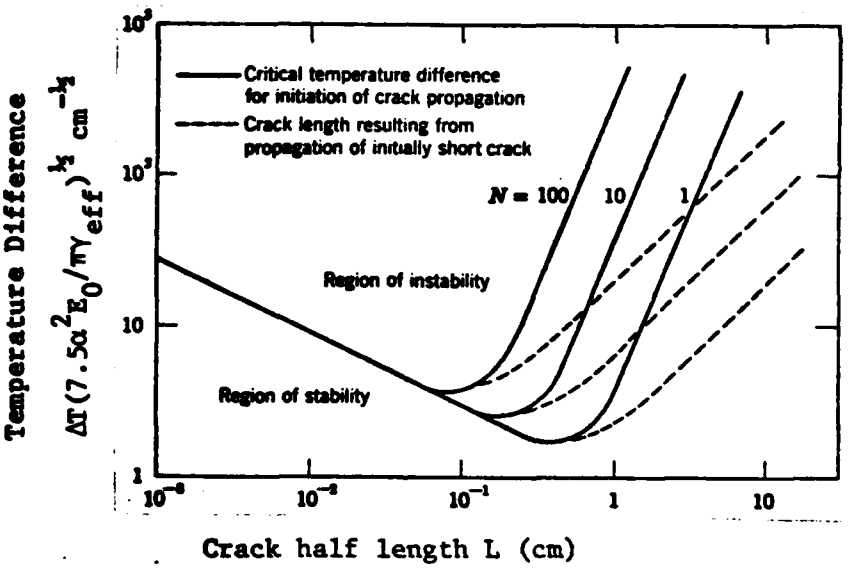

Poisson's ratio assumed to be 0.25.

Figure 2. Thermal Strain Required to Initiate Crack Propagation as a Function of Crack Length and Crack Density N (15).

For initially short cracks, those left of the minima, the rate of energy release after initiation of crack propagation exceeds the surface energy needed for fracture, and the excess energy is transformed

into the kinetic energy of the moving crack. Since the crack still has kinetic energy when it reaches the length given in the expression for ΔT_c, it continues to propagate until the released strain energy equals the total surface energy of fracture (these crack lengths are represented by the dashed lines in Fig. 2). The new crack lengths, being subcritical with respect to the critical temperature difference required for crack initiation, require a finite increase in temperature to become unstable again. Cracks with lengths to the right of the minima will propagate in a quasi-static fashion (15). For a material with small cracks, which propagate kinetically on initiation of fracture, the crack length changes as a function of the severity of the temperature change, Fig. 3. No change in crack length should occur if the thermal stress is less than that needed to initiate fracture. Once the

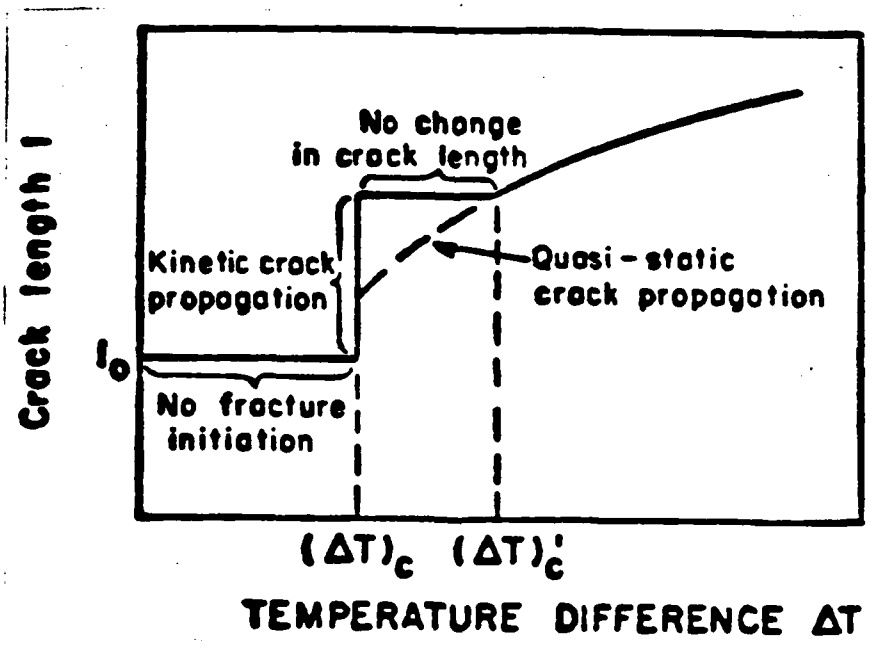

Figure 3. Crack Length as a Function of Temperature Difference ΔT (12, 15).

critical stress for fracture is reached, the cracks propagate rapidly. Over the temperature range of ΔT_c to $\Delta T_c'$ no crack growth occurs because the cracks, which initially propagated when ΔT_c was reached, are now subcritical. The cracks will grow quasi-statically when ΔT is increased beyond $\Delta T_c'$.

Since there are two ways of considering the problem of thermal shock, two principal approaches are taken in designing and selecting materials for thermal shock resistance. One of these approaches is to avoid fracture initiation. This method is used for glasses, porcelain, whitewares, electronic ceramics, etc. In order to avoid fracture initiation by thermal shock, materials should have high values of strength and thermal conductivity and low values of modulus and thermal expansion coefficient. The other approach, which is used for refractory bricks, is to avoid catastrophic crack propagation. To minimize the extent of crack propagation, materials should have high values of modulus and fracture surface work and low values of strength. Therefore, the requirements of modulus and strength for avoidance of crack propagation are directly opposed to those for avoidance of fracture initiation. Choosing material characteristics to deter fracture initiation can, then, have deleterious effects if cracks are initiated because crack propagation will then be enhanced.

Depending on the application, numerous ways exist for improving thermal shock resistance (13, 14). By introducing microstructural heterogeneities to act as stress concentrators in a material, catastrophic crack propagation can be prevented because fracture is induced locally, thus avoiding catastrophic failure since the average stress is kept low.

An example of this might be the introduction of enough cracks of sufficiently large size so that crack propagation takes place quasi-statically. Blunt flaws, such as those resulting from intergranular shrinkage cracking, can improve the resistance to catastrophic failure, while sharp initial cracks from surface impacts can lead to premature failure. In Al_2O_3-TiO_2 ceramics, where tensile strength is not of prime concern, intergranular shrinkage voids improve thermal shock resistance by blunting initially sharp cracks and preventing their propagation. In materials where crack initiation is undesirable, techniques which avoid areas of stress concentration, and designs which avoid restraints and allow for expansion of various parts of the structure, can improve thermal stress resistance. In some cases thermal stresses can be reduced by reducing the size of component parts without loss of utility. By varying material parameters, such as strength, elastic modulus, density, coefficient of thermal expansion, thermal conductivity, purity, etc., thermal shock resistance can be improved through avoidance of crack initiation and/or avoidance of catastrophic crack propagation. The possibility of prestressing ceramic materials also offers an opportunity for increasing thermal stress resistance.

The Thermal Stress Resistance Parameters R, R", and R'''

Numerous thermal stress resistance parameters have been defined (Table I). For any given application only a few of these parameters need be considered. Each of these parameters is a function of certain material constants. In the present study the thermal stress resistance parameters R, R", R''' were considered.

Table I

Summary of Thermal Stress Resistance Parameters and Their Appropriate Thermal Environments

Thermal stress fracture resistance parameters	Literature designation	Thermal environment. The appropriate parameter is used to compare:
$\frac{S_t(1-\nu)}{\alpha E}$	R	a. The maximum allowable temperature difference in body under conditions of steady heat flow.
		b. The maximum allowable temperature difference to which body can be subjected in convective environment for $\beta>>1$.
		c. The maximum allowable temperature gradient in steady state heat conduction in solid containing nonconducting holes or cavities.
$\frac{S_t(1-\nu)k}{\alpha E}$	R'	a. The maximum allowable heat flux through body under conditions of steady heat flow.
		b. The maximum allowable temperature difference to which body can be subjected under convective heat transfer for $\beta<1$.
		c. The maximum allowable heat flux in steady state heat conduction in solid containing nonconducting holes or cavities.
$\frac{S_t(1-\nu)\alpha}{\alpha E}$	R''	a. The maximum allowable rate of surface heating.
$\frac{S_t(1-\nu)}{\alpha\eta}$	R_{cr}	a. The maximum allowable rate of increase of temperature difference across body undergoing thermal stress relaxation by creep.
$\frac{S_t(1-\nu)k}{\alpha\eta}$	R'_{cr}	a. The maximum allowable rate of change of heat flux through body undergoing thermal stress relaxation by creep.
$\left\{\frac{S_t(1-\nu)k}{\alpha E\epsilon}\right\}^{1/4}$	R_{rad}	a. The maximum allowable blackbody radiation to which opaque material can be subjected.
$\left\{\frac{S_t(1-\nu)k}{\alpha E\epsilon(1-F_{\lambda_0})}\right\}^{1/4}$	R_{transp}	a. The maximum allowable blackbody temperature to which semitransparent materials can be subjected the adsorption properties of which can be described as transparent for $\lambda<\lambda_0$ and opaque for $\lambda>\lambda_0$.
$\frac{E}{S_t^2(1-\nu)}$	R'''	a. The minimum in the elastic energy at fracture available for crack propagation.
$\frac{GE}{S_t^2(1-\nu)}$	R''''	a. The minimum in the extent of crack propagation on initiation of thermal stress fracture.
$-\log\left[\frac{S_t^2}{EG}\right]$	T	a. The minimum in the total number of fragments resulting from thermal stress fracture initiation.
$\left[\frac{G}{\alpha^2E}\right]^{1/2}$	R_{st}	a. The maximum allowable temperature difference required to propagate long cracks under severe thermal stress conditions (β, large).
		b. The maximum allowable temperature gradient in bodies containing cracks perpendicular to heat flux.
$\left[\frac{Gk^2}{\alpha^2E}\right]^{1/2}$	R'_{st}	a. The maximum allowable temperature difference required to propagate long cracks for mild thermal stress condtions (β, small).
		b. The maximum allowable heat flux in bodies containing cracks perpendicular to heat flow.

Symbols are defined on the next page (Ref. 17).

Table I (con.)

List of Symbols

α	coefficient of thermal expansion
A	total area of cracks
a	thermal diffusivity
β	Biot's modulus ($\beta = bh/k$)
b	thickness of flat plate, radius of sphere, radius of spherical cavity
C, C'	geometric constants for internally heated hollow cylinders
ε	emissivity
E	Young's modulus of elasticity
η	viscosity
F_{λ_0}	fraction of total energy from blackbody radiation below frequency λ_0
G	surface fracture energy
h	surface heat transfer coefficient
k	thermal conductivity
λ_0	wavelength above which semitransparent ceramic is opaque and below which it is transparent
l	crack half-length
ν	Poisson's ratio
N	total number of cracks, total number of fragments
Q_{max}	maximum heat flow
$\dot{Q}_{max}$	maximum rate of change of heat flow
ρ	Stefan-Boltzmann constant
r_2	outside radius of hollow cylinder
r_1	inside radius of hollow cylinder
S_t	tensile strength
T_{max}	maximum temperature gradient
$\dot{T}_{max}$	maximum rate of change of temperature
ΔT_{max}	maximum temperature difference
$\Delta \dot{T}_{max}$	maximum rate of change of temperature difference
t	time
t^*	time to maximum stress
W_T	total elastic energy

R is a parameter that measures the resistance to fracture initiation and is given by

$$R = \frac{\sigma(1-\nu)}{\alpha E} \qquad (^{o}C) \tag{3}$$

where σ is the bend strength (or more generally the fracture strength), ν is Poisson's ratio, α is the coefficient of thermal expansion, and E is Young's modulus of elasticity. R is a measure of the maximum allowable change in temperature (ΔT) for steady heat flow.

R'' is another parameter for characterizing the resistance to fracture initiation and is represented by

$$R'' = \frac{\sigma(1-\nu)a}{\alpha E} \qquad (cm^{2o}C/sec.) \tag{4}$$

where the symbols have the same meaning as given above, with a being the thermal diffusivity. R'' is a measure of the maximum allowable rate of surface heating.

The parameter R''' is a measure of the resistance of a material to crack propagation damage and can be expressed by

$$R''' = \frac{E}{\sigma^2(1-\nu)} \qquad (1/MPa) \tag{5}$$

where the symbols again have the same meaning as given above. R''' is a measure of the minimum elastic energy at fracture available for crack propagation.

The parameters R, R'', and R''', through the use of shape factors

(18), can be related to $\Delta T_{max.}$, $\dot{T}_{max.}$, and W_T, respectively, where $\Delta T_{max.}$ is the maximum temperature difference, $\dot{T}_{max.}$ is the maximum rate of change of surface temperature, and W_T is the total elastic energy available for crack propagation. The shape factors, which are expressions derived from the specific specimen geometry being considered (and depend only on this geometry), are represented by S, S", and S''' for R, R", and R''', respectively. Therefore, the thermal stress resistance parameters can be given by

$$R = \frac{\Delta T_{max.}}{S} , \tag{7}$$

$$R'' = \frac{\dot{T}_{max.}}{S''} , \tag{8}$$

and

$$R''' = \frac{1}{W_T S'''} . \tag{9}$$

Consequently, if $\Delta T_{max.}$, $\dot{T}_{max.}$, and W_T are known for a specific application, along with the shape factors S, S", and S''' that depend on the component geometry, the resistance parameters can be determined without knowledge of the material constants and properties (σ, ν, α, E, a). Originally, the resistance parameters were defined from the material properties and constants that occur in the expressions derived for $\Delta T_{max.}$, $\dot{T}_{max.}$, and W_T for specific applications. Appendices A, B, and C show, for specific applications, how the thermal stress resistance parameters and shape factors are derived. Although the specific geometries considered in Appendices A, B, and C are not those used in the present study, the derivations shown demonstrate the type of analysis

used to determine the thermal stress resistance parameters and the shape factors.

Reasons Why Accurate Expressions for the 3-D Thermal Stresses in Beams/Bars of Rectangular Cross-Section Cannot Be Developed Completely

In order to analytically determine expressions for the thermal stress resistance parameters R, R", and R''' in terms of $\Delta T_{max.}$, $\dot{T}_{max.}$, and W_T, respectively, and their respective shape parameters S, S", and S''', expressions for the thermal stresses in the specimen(s) of interest must be obtained. Development of exact expressions for the thermal stresses that arise during thermal shock, in beams or bars of rectangular cross-section, is not possible for several reasons. They may be stated as follows: 1) the problem requires a three-dimensional analysis, 2) for ceramic materials edge effects greatly influence failure, and 3) the heat transfer between the beam and its surroundings may change from one test to the next.

A method often used for measuring the thermal stress resistance of ceramics consists of quenching specimens in a medium which is at a different temperature from the initial specimen temperature. Water (19, 20), liquid metals (21), oils (22), fluidized beds (23), or eutectic mixtures of salts (24) are typically used as quenching media. The specimens may initially be at a temperature above or below the temperature of the quenching medium. Typical specimen geometries for such tests are spheres (21, 24) or solid cylinders with circular (19) or square (20) cross-sections (in the present study solid cylinders, bars, with rectangular cross-sections were quenched in room-temperature water).

For a bar of rectangular cross-section dropped into water, heat transfer takes place on all six faces of the specimen. Therefore, to develop expressions for the stresses in the bar, heat flow in the x-, y-, and z-directions must be considered. This makes development of analytical expressions extremely difficult. Finite element or numerical analysis is required for even the two-dimensional case considered by Satyamurthy et al. (25) with heat transfer along directions normal to the faces of an infinitely long solid cylinder of square cross-section. The study conducted by Satyamurthy et al. ignored end effects by assuming an infinitely long cylinder. If end effects are important (as they are in the present study), a two-dimensional finite element analysis will not yield accurate results.

Two types of edge effects, also, add complications to any attempts at predicting the thermal stresses in a bar during quenching. Although the maximum stresses possible will occur at the center of the faces of a bar, the axial stress at the specimen edge will exceed the transverse stress at the center of the faces for times less than the time required to reach the maximum stress (25). Therefore, for the case of a thermal shock in which the maximum stresses significantly exceed the fracture stress, failure will most likely be initiated at a specimen edge rather than at a face center. Specimen defects, such as nicks, scratches, or other flaws, are more likely to be introduced along edges than faces during preparation of specimens with planar faces (25). Thus, specimen defects also tend to make edges more likely fracture initiation sites than faces. Satyamurthy et al. (25) stated that this effect will be enhanced further in stress corrosive environments which will promote

more sub-critical crack growth in flaws at the edges because of the more rapid rise in the magnitude of thermal stress than in the case of the center of the faces. Satyamurthy et al. believe that, for most brittle engineering materials tested in practice, the specimen edge may well be the preferred site of failure.

Finally, changes in the rate of heat transfer can also affect the thermal stresses in a bar. For the study of Satyamurthy et al. (25) dealing with a square-cross-section cylinder, heat transfer was assumed to occur by Newtonian convection, i.e., a rate of heat transfer proportional to the instantaneous temperature difference between the surface and the ambient environment. Satyamurthy et al. assumed heat transfer to be uniform along the length of the cylinder in order to avoid axial heat flow. Consequently, if the heat transfer is non-uniform there will be some variation in the thermal stresses. If thermal shock testing is carried out over a range of temperatures, the heat transfer rate may vary significantly from a test, at one temperature, to another test, at a different temperature. Such an effect is illustrated for a water quenching medium in Fig. 4, in which the changes that occur in the heat transfer rate due to variations in the degree of thermal shock (the magnitude of the change in temperature) are shown. Therefore, for thermal shock testing in water, the rate of heat transfer, depending on the temperature range used, may vary substantially.

Material Properties and Crystal Structure of SiC and BN

SiC. Silicon carbide, SiC, is the only compound of silicon and carbon known to occur in the condensed state. Since both silicon and carbon have similar electronegativity, SiC is completely covalent.

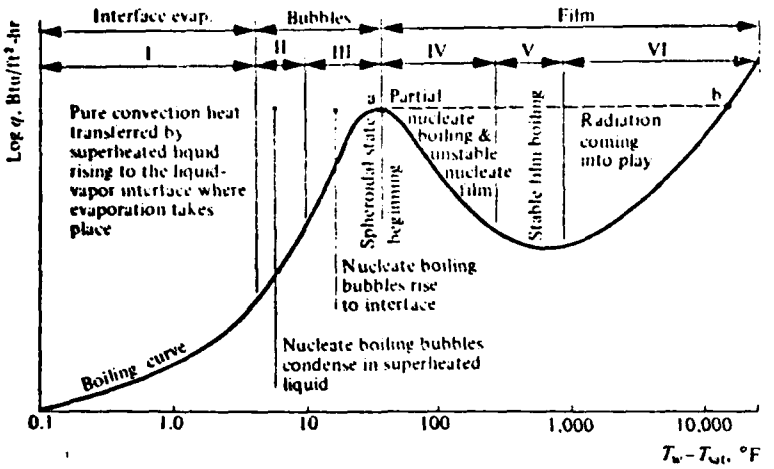

Symbols: q - the rate of heat flow per unit area

T_{sat} - saturation temperature

T_w - surface temperature

Figure 4. Characteristic Boiling Curve (26).

SiC exhibits polytypism, or more generally, polymorphism. Polymorphs are different crystalline modifications of the same chemical substance, and the word polymorphism is used to describe the general relations among the several phases of the same substance without regard to the number of phases being considered (13). Polytypism is a special type of polymorphism in which the different structures assumed by a compound differ only in the order in which a two-dimensional layer is stacked. Silicon carbide can exhibit many polytype crystal structures, several of which commonly occur. These polytypes may all be visualized as being made up of a single basic unit, a layer of tetrahedra which may arbitrarily be chosen as SiC_4 or CSi_4 (27), Fig. 5. The polytypes differ in the orientational sequences by which the layers of tetrahedra are stacked. Although these layers can only be stacked in one of two orientations (a and b, or parallel and antiparallel (28)), the possible

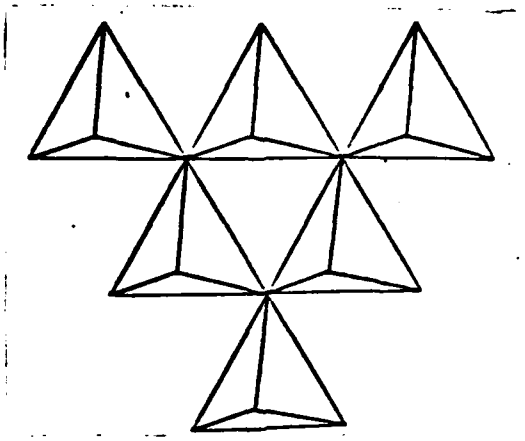

Figure 5. Hexagonal Layers of AB_4 Tetrahedra (28).

sequential combinations of these two orientations over many layers leads to many possible crystal polytypes, Fig. 6. SiC has more polytypic forms than any other material. At least 74 distinct stacking sequences have been found in crystals of SiC, some of which require lattice constants of up to 1500 Å to define the distance over which the stacking sequence repeats (13).

Describing the crystalline polytypes of SiC is accomplished by a system of nomenclature (Ramsdell Notation) that assigns a number

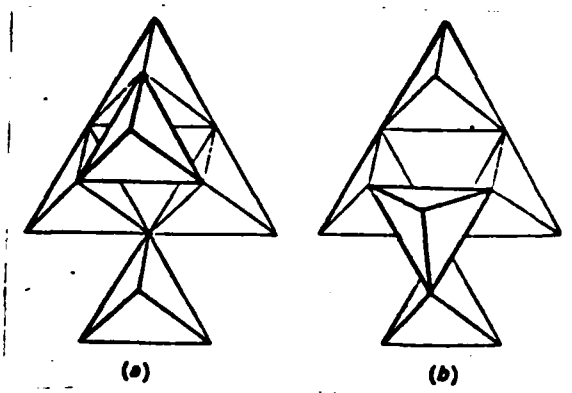

Figure 6. Orientation of Tetrahedra in Successive Hexagonal Layers, (a) Parallel, (b) Antiparallel (28).

corresponding to the number of layers in the unit cell and a letter suffix designating the crystal symmetry. The possible crystal symmetries are cubic (C), hexagonal (H), and rhombohedral (R). The structures of the common SiC crystalline polytypes, those of 3C, 4H, 6H, and 15R, have a, aabb, aaabbb, and $(aaabb)_3$ layer sequences, respectively (28) (the 2H form is also a common polytype). Although a number of theories have been developed to explain the long range order or polytypism in SiC, the numerous crystal structures are most easily explained by Shaffer (28) on the basis of a screw dislocation growth mechanism.

The cubic 3C polytype is usually referred to as beta silicon carbide, β-SiC. All of the other polytypes are collectively referred to as alpha silicon carbide, α-SiC. Although β-SiC may exist at all temperatures up to decomposition, it usually transforms to one of the alpha polytypes at high temperatures. Doping β-SiC with different elements (or adding different elements to β-SiC), such as boron and/or nitrogen, tends to favor the stabilization of certain alpha polytypes. Generally, the transformation of β to α silicon carbide is not reversible, except under certain conditions.

A listing of some of the material properties for SiC is given in Table II. When possible, the data for hot-pressed SiC was chosen.

BN. Boron nitride (BN), which has three different crystalline structures, is one of the most important nitrides for engineering applications. The hexagonal (alpha) form of boron nitride is soft and machinable, similar in structure and properties to graphite, but is an electrical insulator and is more oxidation resistant than graphite

Table II

Material Properties and Constants for SiC

E, Young's Modulus of Elasticity	0.428 - 0.448 X 10^6 MPa
σ_b, Bend Strength	662 MPa
a, Thermal Diffusivity	0.3448 $cm^2/sec.$
α, Coefficient of Thermal Expansion	4.32 X 10^{-6} $^oC^{-1}$ for 24^o - 871^oC 5.40 X 10^{-6} $^oC^{-1}$ for 538^o - 2204^oC
ρ, Density	3.21 gm/cm^3 for β-SiC 3.208 gm/cm^3 for 6H α-SiC
ν, Poisson's Ratio	0.17

(29). At very high pressures and temperatures, alpha BN can be converted to an extremely hard, zinc-blende cubic (beta) form. The properties of α-BN are sensitive to crystallographic orientation because α-BN crystals are highly anisotropic. Alpha boron nitride has a layer structure in which the atoms in the basal plane are held together by strongly directed covalent bonds in a hexagonal array (the graphite structure), Fig. 7. In contrast, the bonds between layers are weak van der Waals forces so that the structure has very strong directional properties (13). The third form of BN, which has a hexagonal wurtzite-type structure that forms under high pressure, is metastable under all conditions (a non-equilibrium phase). Both cubic β-BN and the metastable hexagonal form are similar crystallographically, but the two structures have greatly different mechanical properties, the metastable hexagonal form being much tougher or impact resistant than the cubic form (30).

A listing of some of the material properties for BN is given in

Table III. When possible, the data for hot-pressed BN was chosen.

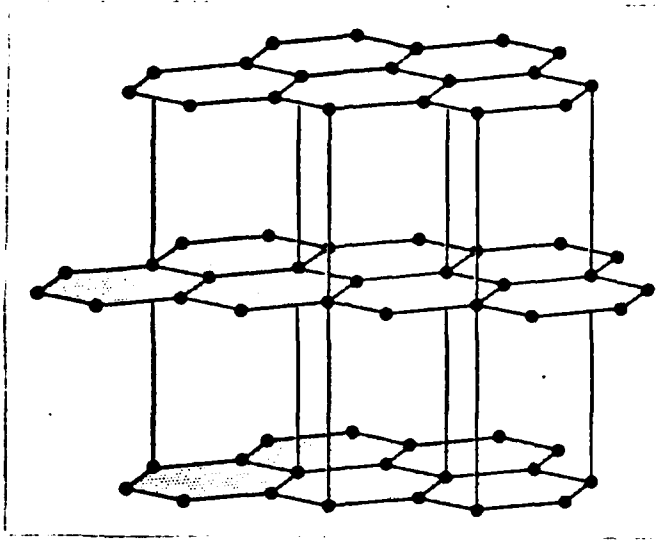

Figure 7. Graphite Structure of Hexagonal Alpha BN (13).

Table III

Material Properties and Constants for α-BN

	Parallel to Hot-Pressing Direction	Perpendicular to Hot-Pressing Direction
E, Young's Modulus of Elasticity	0.041 - 0.097 X 10^6 MPa	0.041 - 0.103 X 10^6 MPa
σ_b, Bend Strength	48 - 97 MPa	41 - 110 MPa
a, Thermal Diffusivity	0.0924 cm^2/sec.	0.1724 cm^2/sec.
α, Coefficient of Thermal Expansion	negative for 38° - 998°C 1.2 X 10^{-6} $°C^{-1}$ for 998°C - 1758°C	0.7 X 10^{-6} $°C^{-1}$ for 38° - 998°C 3.2 X 10^{-6} $°C^{-1}$ for 998° - 1758°C
ρ, Density	2.28 ± 0.01 gm/cm^3	2.28 ± 0.01 gm/cm^3
ν, Poisson's Ratio	0.23	0.23

III. Material and Experimental Procedures

Material

The materials used for this study were commercially available silicon carbide (SiC) and boron nitride (BN) powders. The SiC powder was a high purity, sinterable, beta silicon carbide produced by Hermann C. Starck, Inc. (No. S 1626). The BN powder had an average particle size of one micron and was approximately 99.5 percent pure. It was produced by Cerac, Inc. (No. B-1084). The impurities in the powders were determined by spectrographic analysis; the impurities in the SiC and BN powders are given in Tables IV and V.

Table IV

Impurity Content in SiC Powder

All Concentrations Are in Wt. PPM

B	5700
Al	1300
Fe	230
Na, Zn, W	each < 200
Nb	< 100
Ti, Ca	each 20
Sn, Pb, Ni, Cr, Mo, Zr, V, Co	each < 20
Mg, Mn	each 10
Cu	5

Experimental Procedures

Specimen Preparation. The specimens used for the experimental testing were prepared from the SiC and BN powders described above. To

Table V

Impurity Content in BN Powder

All Concentrations Are in Wt. PPM

Na, Zn, Nb, W.....each < 1000

Ti, Mo, Zr, V.....each < 200

Si.....100

Co, Cr.....each 100

Al, Fe, Ca.....each 60

Mn, Sn, Pb, Ni, Cu.....each < 20

Mg.....10

prepare the powders for hot-pressing (see-below), the required amounts of each powder for the different specimens were calculated, based on the densities of the powders and the size of the desired specimen, and weighed, using Mettler and Chemical Rubber Company analytical balances. After weighing the required amounts of powder for a sample, the SiC and Bn powders were mixed for four hours in a U.S. Stoneware ball mill, using iso-propyl alcohol and Si_3N_4 "balls" in a plastic jar. Once thoroughly mixed, the powders were dried for several hours at 75°C in a Blue M Electric Company oven to evaporate the alcohol.

A two-inch (inside diameter) graphite die was used for hot-pressing with Grafoil as a lubricant. The Grafoil (produced by Union Carbide) also served to keep the powders from reacting with the die walls and plungers. The powders were initially cold-pressed at 6.59 MPa with a Carver laboratory press to compress the powders and to aid in handling of the assembled die/plunger apparatus. All of the specimens fabricated were hot-pressed at 34.48 MPa using a Vacuum Industries,

Inc. hot press. Six specimens were hot-pressed; five were pressed at 2000°C and the sixth was pressed at 1950°C. The specimens hot-pressed were 0, 8.8, 17.9, and 27.2 volume percent (vol. %) BN (0, 10, 20, and 30 mole percent BN), the remainder of each specimen being SiC. Of the six specimens produced, two were 0 vol. % BN and two were 17.9 vol. % BN. After removal from the die, the surfaces of the specimens were ground, with a 70-micron diamond wheel on Buehler Ltd. and Fisher Scientific polishing machines, to clean off any material (premarily Grafoil) adhering to the surfaces. Finally, the test pieces, bend and thermal shock bars, were cut from the hot-pressed specimens using a K.O. Lee Company saw/grinder. In order to perform the machining, the specimens were mounted with epoxy on glass and/or metal specimen holders. Of the six specimens, five were cut so that the large face of the test bars was perpendicular to the direction of the hot-pressing load (Fig. 8); one of the 17.9 vol. % BN specimens was cut with the large faces of the test bars parallel to the hot-pressing direction, in order to observe possible anisotropy in the composites.

The bend and thermal shock bars were prepared by standard ceramographic techniques so that light optical pictures could be taken, and so that bend strength and thermal shock resistance measurements could be made. The edges of the bars were bevelled and all four sides of each bar were ground consecutively on 240, 320, 400, and 600 grit SiC paper using water as a lubricant/coolant. The bars were then polished with 15-, 9-, and 6-micron diamond paste on selected silk cloths with Metadi Fluid as a lubricant/coolant (Note: all polishing and grinding materials were produced by Buehler Ltd.). Only three

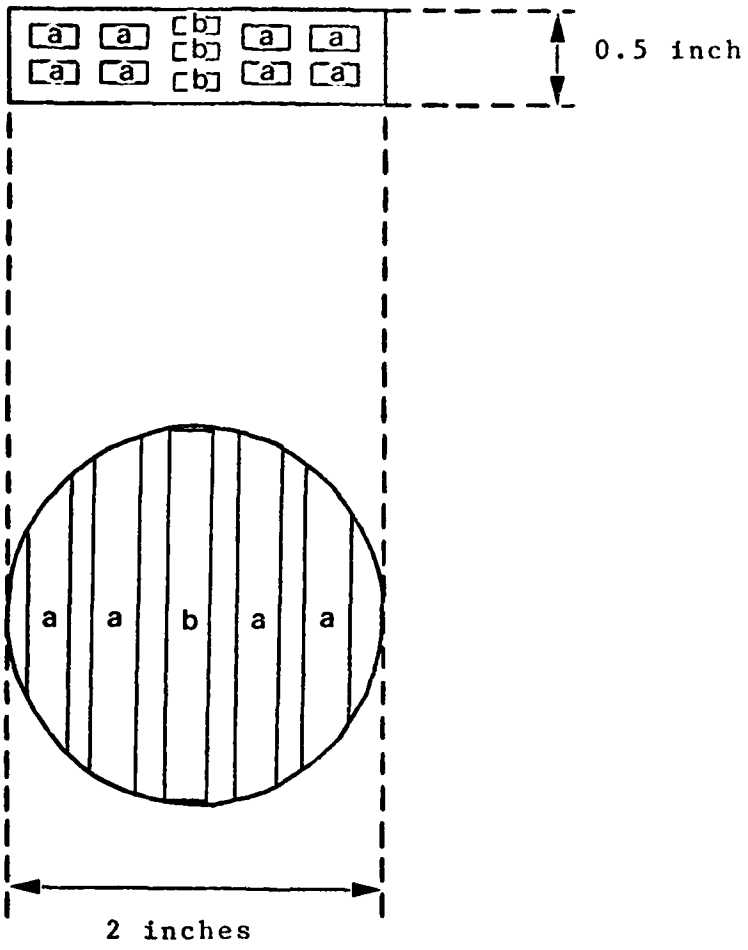

a - Bend Bars (0.125 in. X 0.250 in.)

b - Thermal Shock Bars (0.090 in. X 0.250 in.)

Figure 8. Orientation of Test Bars in Hot-Pressed Specimens, Shown at Actual Size.

sides of the bend bars (those on the tensile-stress side) were polished with 9- and 6-micron finish. The compressive side of the bend bars was not polished as finely because failure of the bend bars occurs in tension, and, therefore, a fine polish was not required on the compressive side. Grinding and polishing was accomplished using Buehler Ltd. and Fisher Scientific polishing machines.

Microstructural Characterization. The microstructures of the six hot-pressed specimens were characterized by light microscopy (LM), scanning electron microscopy (SEM), x-ray diffraction (XRD) analysis, and density measurements.

The bulk densities of the specimens were determined using an ASTM standard test method (31). After oven drying (using a Blue M Electric Company oven) at 150°C for approximately three hours and cooling in a desiccator, the specimens were weighed. Then the specimens were boiled in distilled water and weighed while suspended in distilled water. Finally, the specimens were blotted dry and weighed again. The densities of the specimens were then determined from the data obtained from the different weight measurements, which were conducted according to the ASTM standard test method (31).

X-ray diffraction analysis of the phases present in the hot-pressed specimens and in the SiC and BN powders was accomplished with a Philips Electronic Instruments diffractometer using Ni-filtered Cu K_α radiation. The powder specimens were mounted on glass microscope slides using clear nail polish to bind the powders in place. The mounted powder samples and pieces of the hot-pressed specimens were analyzed using standard x-ray techniques (32).

Light microscopy was used to characterize the microstructures of the six hot-pressed specimens. Light optical pictures were obtained using a Bausch & Lomb Optical Company Research II Metallograph (microscope) with a green filter. Polished bend and thermal shock bars were used for LM microstructural analysis.

An AMR Model 1000 Scanning Electron Microscope was employed to characterize the microstructures of the hot-presses specimens as well as to examine the fracture surfaces of broken bend bars. Specimen preparation for the SEM studies involved grinding specimens to the required size, mounting the specimens on sample holders, coating the specimens with carbon and gold to prevent charging in the microscope, and applying a small amount of silver paint to the base of the specimens to aid electron flow. Pictures of the microstructures of the six hot-pressed specimens and of possible fracture initiation sites in several of the fractured bend bars were obtained using standard SEM techniques.

Experimental Testing. The experimental testing involved conducting four-point bend tests, at room and elevated temperatures, and water-quench thermal shock tests. Thermal shock bars from each of the six hot-pressed specimens were also sent to the IIT (Illinois Institute of Technology) Research Institute (Chicago, Illinois) for additional testing. This testing involved developing thermal expansion curves, determing Young's moduli and coefficients of thermal expansion, and measuring the thermal shock resistance by a different technique from that used in the present study. Thermal diffusivity data from a study conducted at Wright-Patterson AFB (Ohio) and Virginia

Polytechnic Institute and State University (Blacksburg, Virginia) (33) was also used in conjunction with the data obtained in the present study.

Thermal shock testing was conducted using a Blue M Electric Company Lab-Heat Muffle Furnace. Thermal shock bars were heated in air to the desired temperature and then allowed to soak at this temperature for 30 minutes, in order for the temperature in the bar to reach equilibrium (for all of the specimens tested, the initial temperature used was 250°C). Then the bars were quenched in distilled water at room temperature (approximately 22°C), by dropping them into a two liter beaker filled with water. After the bars cooled and were dried off, they were examined for surface cracks using a Bausch & Lomb Optical Company binocular light microscope. The above procedure was repeated, as many times as required, until the bars showed evidence of cracking. The appearance of cracks was used as the failure criterion. Each temperature cycle was conducted at a temperature 25°C above that of the previous cycle.

Flexure strength was measured by four-point bend tests using an Instron testing machine with a Brew furnace. All bend tests were conducted at a cross-head loading rate of 0.005 cm per minute. Tests were run at room temperature and at 1000°, 1250°, and 1500°C. For the elevated temperature tests, bend bars were allowed to soak at the desired test temperature for 30 minutes, in order for the temperature in the bar to reach equilibrium. In all of the bend tests, the bend bars were placed in the test fixture with the tensile side(s) of the bars being the more finely polished side(s).

IV. Results and Discussion

Characterization of the Microstructure of the SiC-BN Composite Specimens

The microstructures of the six silicon-carbide/boron-nitride composite specimens were characterized by x-ray diffraction (XRD) analysis, density determinations, light microscopy (LM), and scanning electron microscopy (SEM). The six specimens were made with the following compositions: 0, 8.8, 17.9, and 27.2 volume percent BN (or 0, 10, 20, and 30 mole percent BN) with the remainder consisting of SiC. Note that the impurities in the BN and SiC starting powders (presented earlier) are considered as BN and SiC for the purpose of calculating percent BN compositions (i.e. the impurities are considered as being of negligible amounts).

Of the six compositions used, two were 0 vol. % BN and two were 17.9 vol. % BN. The two 0 vol. % BN specimens were hot-pressed at different temperatures, 2000° and 1950°C, to see what changes would occur in the material properties and constants. Changing the processing temperature, within the range considered in this study, primarily changes the grain size of the specimens. The two 17.9 vol. % BN specimens were both hot-pressed at 2000°C, but the test bars (bend bars and thermal shock bars) in one were cut from the hot-pressed specimen at an orientation 90° different from those in the other specimen. Thus, the effect of anisotropy arising from the hot-pressing operation could be assessed from the two 17.9 vol. % BN specimens. Unless stated otherwise, the 0 vol. % BN specimen hot-pressed at 1950°C will be designated as 0% vol. % BN and the 17.9 vol. % BN specimen, whose test bars were cut out

of the hot-pressed billet (specimen) at an orientation 90° to those cut out of the other billets, will be designated as 17.9P vol. % BN.

The densities of all six specimens were measured and compared to their theoretical values. In all cases the measured values were close to the theoretical values. The highest percentage of porosity in any of the specimens was determined to be 2.6 %. Thus, all of the specimens were at least 97.4 % dense. Data dealing with the densities of the six specimens are given in Table VI.

Table VI

Densities of the SiC-BN Composites

BN Content		Density (gm/cm^3)		% Porosity	% Dense
Volume %	Mole %	Measured	Theoretical		
0.0	0	3.18	3.21	0.9	99.1
0.0F	0F	3.21	3.21	0.0	100.0
8.8	10	3.06	3.13	2.3	97.7
17.9	20	2.96	3.04	2.6	97.4
17.9P	20P	2.99	3.04	1.8	98.2
27.2	30	2.88	2.96	2.5	97.5

X-ray diffraction analysis of the six hot-pressed specimens and the two starting powders was used to determine which BN and SiC phases were present in the samples. The SiC powder used in the fabrication of the hot-pressed specimens was determined to be beta SiC, which has a face-centered cubic structure (3C). The BN starting powder was characterized as alpha BN, which has a hexagonal graphitic structure. All of the SiC-BN hot-pressed specimens were found to have alpha BN and

multiple SiC phases (the 0 and OF vol. % BN specimens, obviously, did not show evidence of alpha BN). The multiple SiC phases in the specimens included β-SiC and the 2H, 4H, 6H, 15R, and 21R forms of α-SiC. Other polytypes of SiC may have been present, but the amounts (percentages) of these other polytypes were too small to yield x-ray peaks during the diffractometer scans. Thus, in all of the hot-pressed specimens, multiple phases of SiC were observed, including cubic, hexagonal, and rhombohedral forms. In the specimens containing BN, the hexagonal α-BN form was observed.

Light microscopy was used to characterize the microstructures of the hot-pressed specimens after representative pieces had been ground and polished. In all six specimens small amounts of porosity (voids) were visible. The BN phase was observed to be relatively uniformly distributed throughout the SiC matrix. The BN particles in the specimens were oriented in a direction perpendicular to the hot-pressing direction, the direction along which the load had been applied during hot-pressing. The microstructure of the 8.8 vol. % BN-SiC specimen is shown both parallel to and perpendicular to the hot-pressing direction in Fig. 9. When observing this specimen parallel to the hot-pressing direction, the BN particles appear to be randomly oriented, but when observed perpendicular to the hot-pressing direction, the BN particles are seen to be oriented perpendicular to the hot-pressing direction. This phenomenon was observed for all four of the specimens containing BN. The dark areas in Fig. 9 are BN particles, voids where BN had existed but was pulled out of the specimen during polishing, and porosity. By comparison with the 0 and OF vol. % BN specimens, the porosity

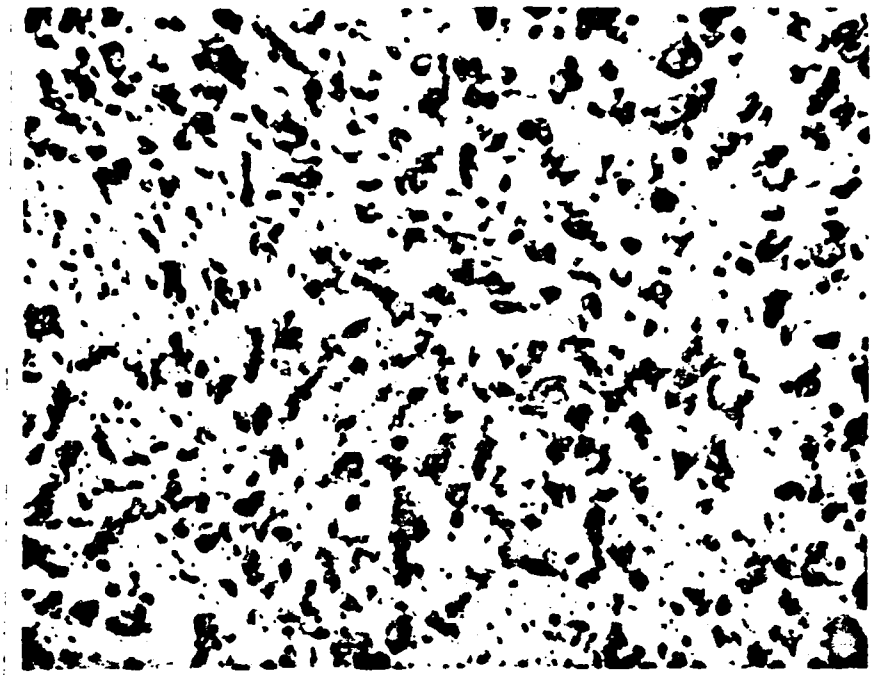

a

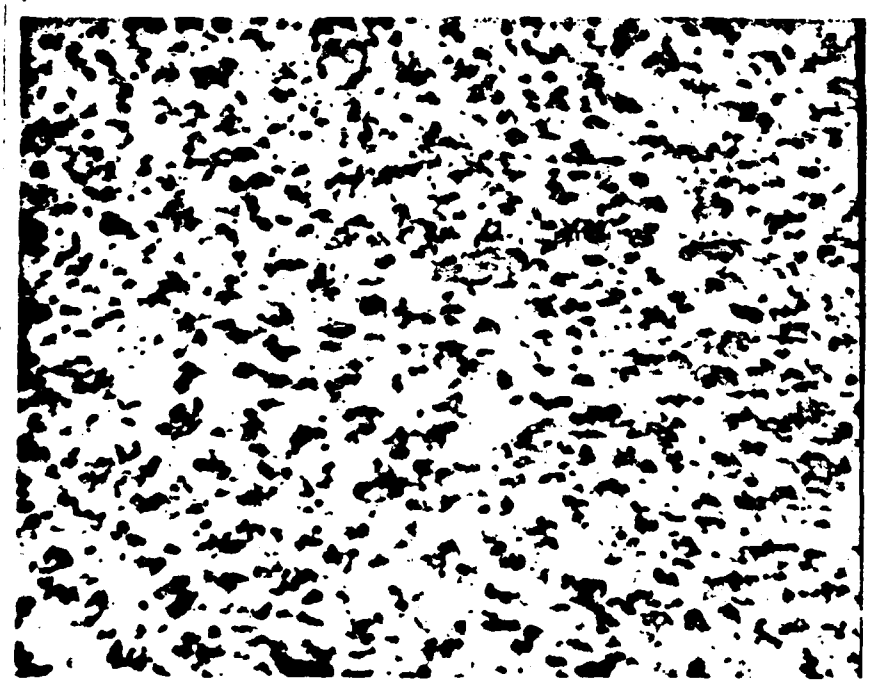

b

Figure 9. LM Micrographs of the 8.8 Vol. % BN Specimen (a) Parallel to and (b) Perpendicular to the Hot-Pressing Direction (650X).

in the figure tends to be the smaller of the darks areas. Thus, from the LM micrographs, it can be seen that hot-pressing tends to orient the BN particles roughly perpendicular to the direction of the applied hot-pressing load.

Scanning electron microscopy was also used to characterize the microstructures of the hot-pressed specimens. SEM analysis was conducted using the fracture surfaces of broken bend bars. In the specimens containing BN, the boron nitride particles were observed as thin plate-like structures oriented with the plane of the plates approximately perpendicular to the hot-pressing direction. As observed by SEM (and also by LM), the BN particles, which are initially plate-like particles in the powder form, tend to orient themselves perpendicular to the applied load. Thus, some degree of anisotropy in the composites is introduced by the hot-pressing process, which orients the BN particles. The microstructures of the six hot-pressed specimens are shown in Figs. 10-15. In all of the specimens, fine roughly equiaxed particles can be seen. These particles are impurities in the composites and particles that have adhered themselves to the fracture surface. The OF vol. % BN-SiC specimen was found to have a finer grain size than the 0 vol. % BN-SiC specimen. The finer grain size occurred because the OF vol. % specimen was hot-pressed at a temperature 50^{o}C below that at which the other specimens were hot-pressed. By comparing Figs. 10 and 11, it can be seen that the grain size is much finer in the OF vol. % BN-SiC specimen (Fig. 11) than in the 0 vol. % BN-SiC specimen. The finer grain size, of the specimen pressed at the lower temperature, results in a rougher appearing fracture surface than that of the specimen with

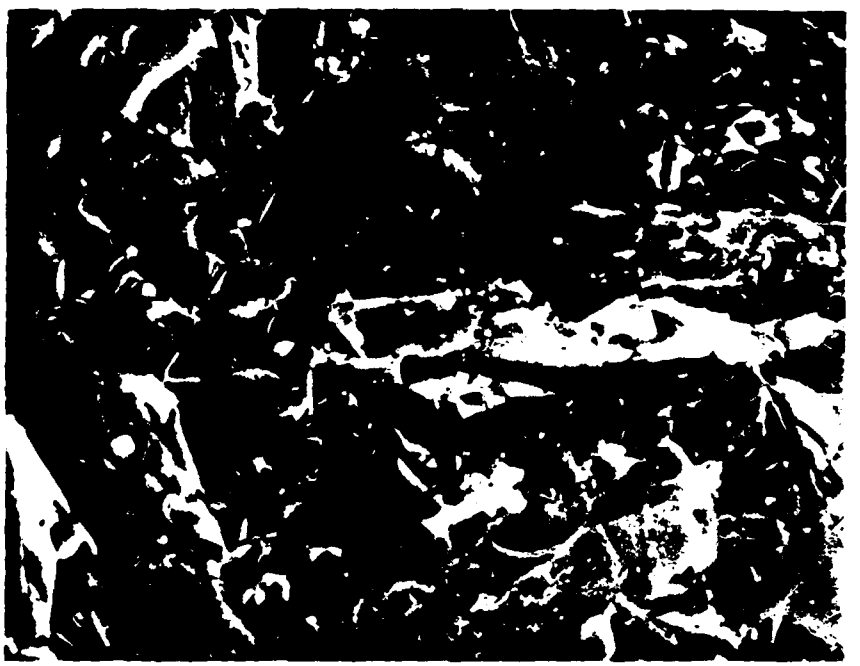

a

b

Figure 10. SEM Micrographs of the 0 Vol. % BN Specimen ((a) 1,000X and (b) 2,000X).

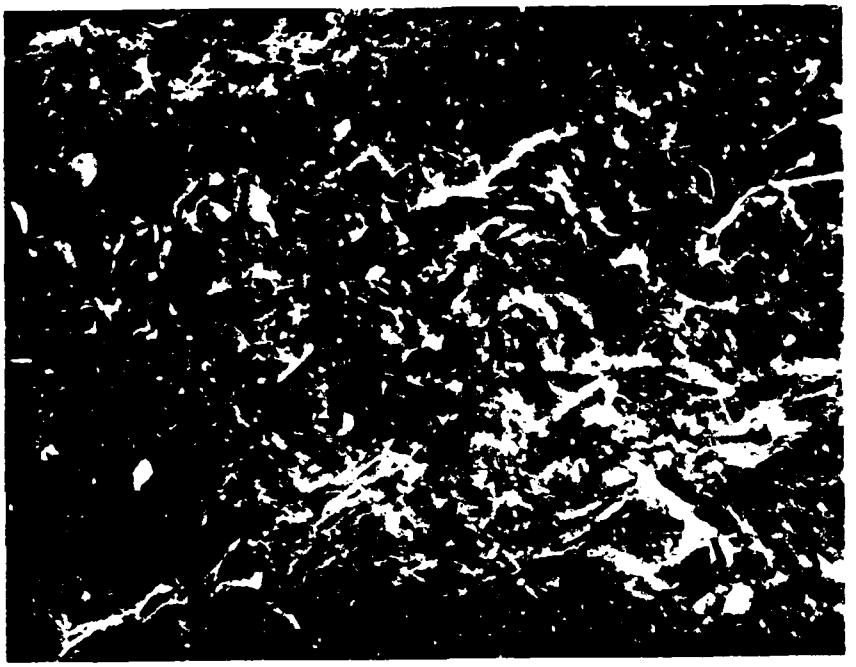

a

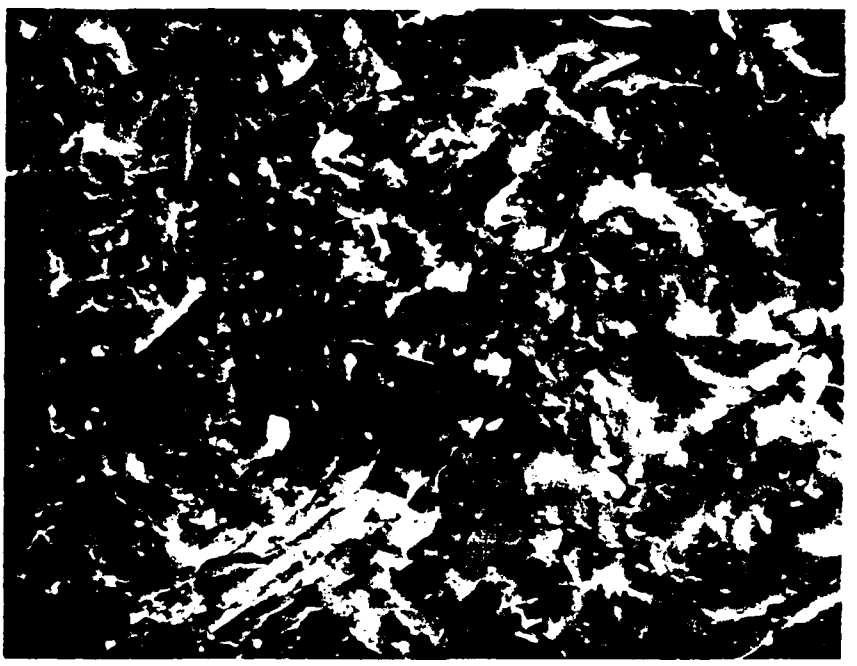

b

Figure 11. SEM Micrographs of the 0F Vol. % BN Specimen ((a) 1,000X and (b) 2,000X).

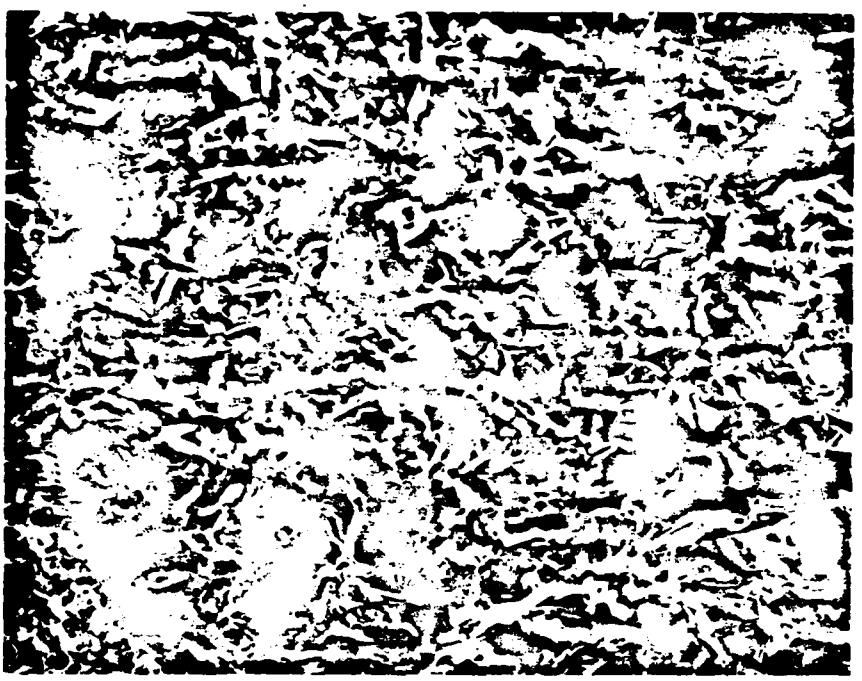

a

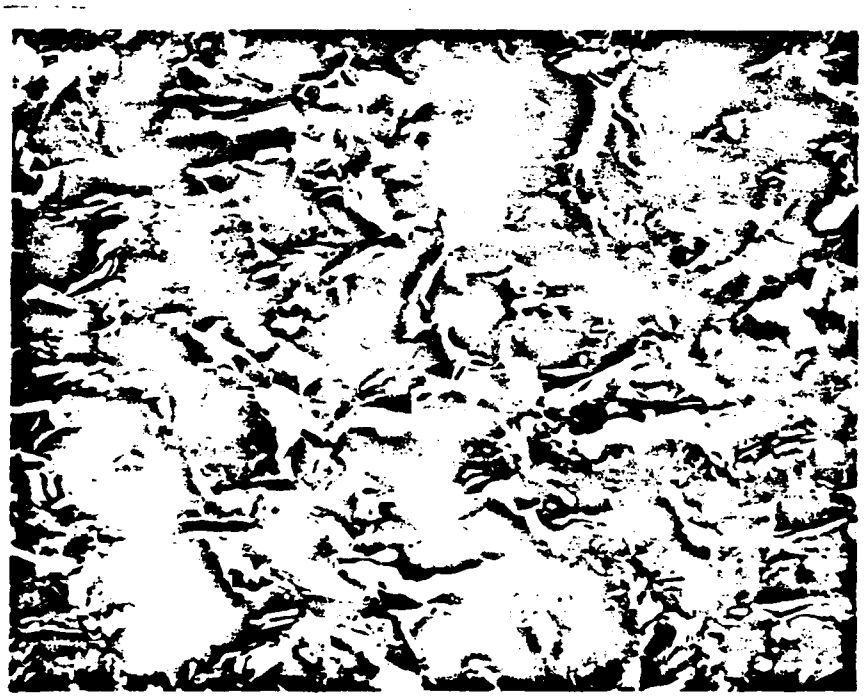

b

Figure 12. SEM Micrographs of the 8.8 Vol. % BN Specimen ((a) 1,000X and (b) 2,000X).

a

b

Figure 13. SEM Micrographs of the 17.9 Vol. % BN Specimen ((a) 1,000X and (b) 2,000X).

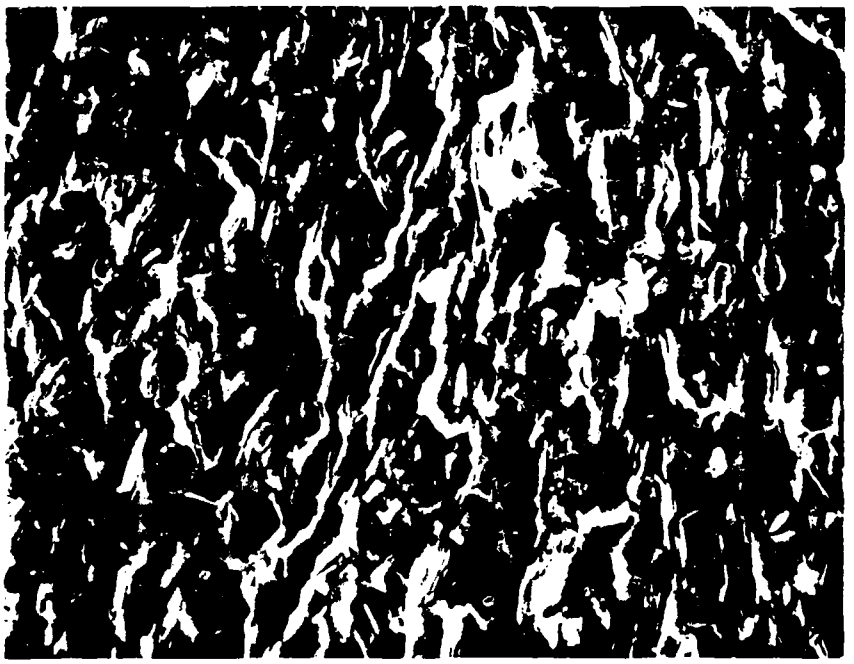

a

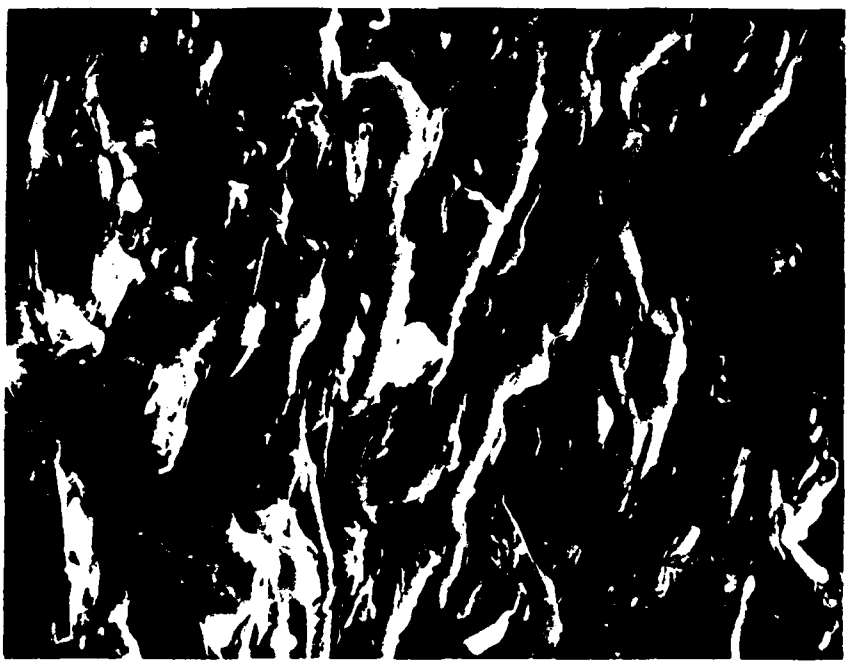

b

Figure 14. SEM Micrographs of the 17.9P Vol. % BN Specimen ((a) 1,000X and (b) 2,000X).

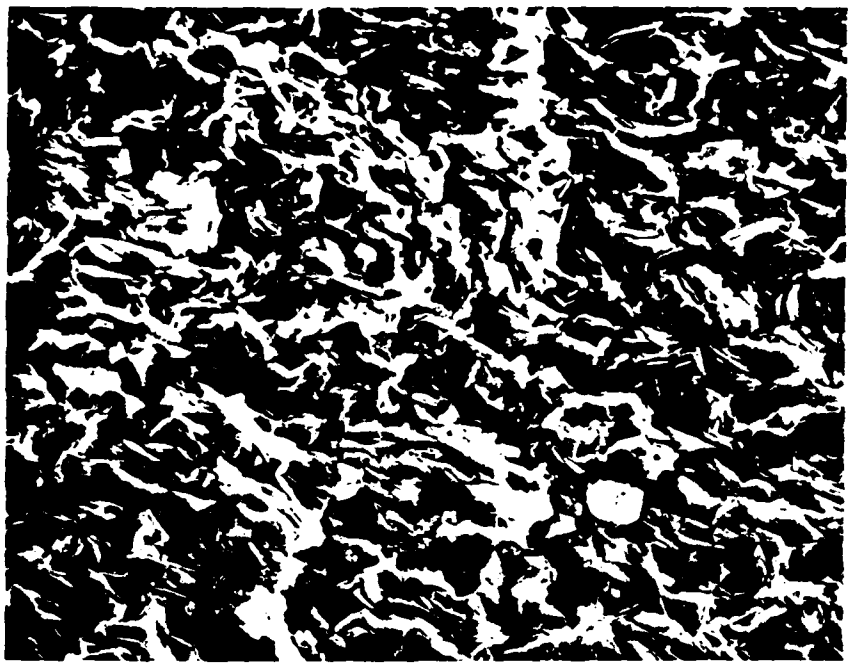

a

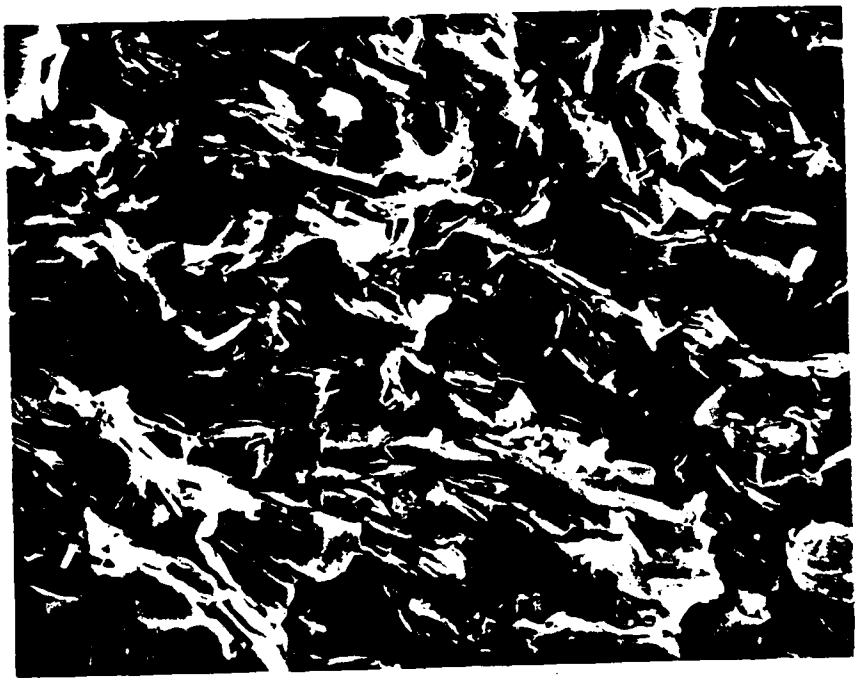

b

Figure 15. SEM Micrographs of the 27.2 Vol. % BN Specimen ((a) 1,000X and (b) 2,000X).

the coarser grain size, which has a much smoother appearing fracture surface. In all of the figures, the micrographs are oriented such that the vertical direction corresponds to the direction normal to the largest faces of the test bars. Thus, in the specimens containing BN particles (Figs. 12-15), the plane of the BN plates is roughly parallel to the plane of the largest faces of the test bars in all but the 17.9P vol. % BN-SiC specimen, whose BN particles are oriented 90^{o} from the orientation of the BN particles in the test bars of the other specimens. As mentioned earlier, the 17.9P vol. % BN-SiC specimen was machined differently so that possible anisotropy effects could be observed.

Influence of BN Content on the Material Constants of the Composite Specimens

Changes in the material constants of the composite specimens, as functions of the BN content, were characterized. The effects, on the coefficient of thermal expansion and Young's modulus of elasticity, were determined for the SiC-BN particulate composites by experimental methods. Data for the changes in thermal diffusivity with changing BN content were taken from a study on the thermal diffusivity anisotropy of SiC-BN composites (33). Values of Poisson's ratio for the different specimens were estimated from the values for pure SiC and pure BN.

For all six of the hot-pressed specimens, values of the linear expansions at $1000^{o}C$ and the coefficients of thermal expansion were determined. The linear expansion, which can be represented by $\Delta L/L$ (where L is the length of the specimen) was used to determine the mean coefficient of thermal expansion, which is given by

$$\bar{\alpha} = \frac{\Delta L}{L \Delta T} \quad (^{o}C^{-1}) \tag{10}$$

where ΔT is the temperature range over which $\bar{\alpha}$ is defined. Although the coefficient of thermal expansion is a function of temperature, it is generally approximated by the mean value for sufficiently limited temperature ranges. Therefore, unless stated otherwise in the following sections, the values of the coefficients of thermal expansion of the composite specimens are actually the mean values. Both the mean coefficients of thermal expansion and the values of the linear expansions were observed to be relatively insensitive to changes in the BN content (Table VII).

Table VII

Linear Expansions and Mean Coefficients of Thermal Expansion for the SiC-BN Composites

Composite BN Content (vol. %)	Linear Expansion at 1000°C (%)	Mean Coefficient of Thermal Expansion (20°-1000°C) ($^{o}C^{-1}$)
0.0	0.412	4.20
0.0F	0.440	4.49
8.8	0.440	4.49
17.9	0.439	4.48
17.9P	0.417	4.26
27.2	0.430	4.39

Changing the BN content, though, was found to have a significant effect on the Young's moduli of elasticity of the specimens. As the BN

content increased, the Young's modulus decreased. Similar results were obtained by Mazdiyasni and Ruh (34) for a study dealing with Si_3N_4-BN composites; increases in the BN content of the specimens, from 0 to 12.5 weight %, were found to decrease the Young's moduli of the composites. For the two 0 vol. % BN specimens (0 and 0F), the specimen with the finer grain size was found to have a slightly greater modulus of elasticity. The fact that the moduli of the two 0 vol. % BN specimens are similar is what one would expect, since Young's modulus is independent of grain size. Of the two 17.9 vol. % BN specimens (17.9 and 17.9P), the specimen, whose test bars were cut at an orientation 90° different from the others, was found to have a slightly higher modulus than the other 17.9 vol. % specimen. The Young's moduli of the specimens and estimated values of the Poisson's ratios are given in Table VIII. The Poisson's ratios were determined by linearly extrapolating between the value of 0.17 for SiC and the value of 0.23 for BN.

The thermal diffusivity (a) is the ratio of the thermal conductivity (k) to the heat capacity per unit volume (ρc_p). Data for the thermal diffusivity of the composites was taken from a study by Ruh et al. (33). This data should be, to a good approximation, equal to the actual values of the specimens used in the present study because the composites used in the two studies differ only slightly in the initial BN particle size and the hot-pressing temperature (in the study of Ruh et al. (33) the BN particles were 15 microns in size and the specimens were pressed at $2100^{\circ}C$, in the present study the BN particles were 1 micron is size and the specimens were pressed at $2000^{\circ}C$). The thermal diffusivity (Table IX) remains relatively constant, as the BN content

Table VIII

Young's Moduli of Elasticity and Poisson's Ratios for the SiC-BN Composites

Composite BN Content (vol. %)	Young's Modulus of Elasticity[a] (MPa)	Poisson's Ratio[b]
0.0	0.4028×10^6	0.17
0.0F	0.4186×10^6	0.17
8.8	0.3162×10^6	0.18
17.9	0.2966×10^6	0.18
17.9P	0.2986×10^6	0.18
27.2	0.2614×10^6	0.19

(a) IIT Research Institute flexural resonant frequency method.

(b) Determined by linear extrapolation.

Table IX

Thermal Diffusivities of the SiC-BN Composites

Composite BN Content (vol. %)	Thermal Diffusivity (33) (cm^2/sec.)	
	Perpendicular to H.P.D.[a]	Parallel to H.P.D.[a]
0.0	0.4328	0.3994
8.8	0.3693	0.3065
17.9	0.3620	0.2379
27.2	0.3995	0.2200

(a) H.P.D. = Hot-Pressing Direction

is increased, when measured perpendicular to the hot-pressing direction (the direction corresponding to the plane of the BN plates), but drops drastically when measured parallel to the hot-pressing direction (the direction roughly normal to the plane of the BN plates) (33). This anisotropy is due both to the orientation of the BN plates in the hot-pressed specimens and to the anisotropy associated with pure BN.

Thermal Shock Behavior of the SiC-BN Composites

Thermal shock behavior can be characterized in either of two ways, quenching a body into a medium of lower temperature or into one of a higher temperature (12). In the case when the media temperature is lower than the temperature of the body, the surface of the body contracts but is constrained by the bulk and tensile stresses arise in the surface. For stress equilibrium, the surface tensile stress must be balanced by compressive stresses in the interior. For the other situation, that in which the media temperature is higher than the temperature of the body, the converse is true; compressive stresses arise in the surface of the body and the interior is in tension. Since ceramic materials are generally much weaker in tension than in compression, failure usually initiates from the surface during cooling or from the center during heating (12, 13). Failure during rapid cooling occurs more often than during rapid heating, though, because of the presence of flaws on the surface and their interaction with the tensile stresses. Thus, thermal shock tests are generally carried out by quenching a body into a media of lower temperature.

The SiC-BN composites were subjected to two sets of thermal shock tests to characterize their thermal shock behavior. Both tests were

water quench tests in which the water was at a lower temperature than the composites. Different methods were used to determine when failure occurred; one method involved only optical observations, while the other method involved both optical observations and internal friction measurements. The results of both tests showed that increasing the BN content increased the maximum change in temperature (ΔT) that the composites could withstand (Fig. 16). The results differed, somewhat, as to the effect of grain size and BN-plate orientation on the thermal shock behavior (Table X). When comparing the coarse- and fine-grained 0 vol. % BN specimens, one of the tests showed grain size had no effect, while the other showed that the fine-grained specimen (OF vol. % BN) failed at a lower ΔT than the coarse-grained specimen (0 vol. % BN). This is opposite of what one would expect; fine-grained materials usually have higher strength than coarse-grained materials (of the same composition) and, therefore, higher values of R and R" (and therefore higher values of ΔT). The lower values of R or ΔT are most likely caused by the existence of residual stresses in the fine-grained specimens (see next section). Comparisons of the two 17.9 vol. % BN specimens, whose BN-particles were oriented differently, showed different results for the two tests; one of the tests showed changing the orientation increased the ΔT by 50°C, while the other test showed a decrease of 50°C for such an orientation change.

Determination of the Effect of BN on the Bend Strength of SiC

The influence of BN content on the four-point bend strength of the composites was examined. Fracture surfaces were also characterized and possible fracture initiation sites were studied. The bend strength,

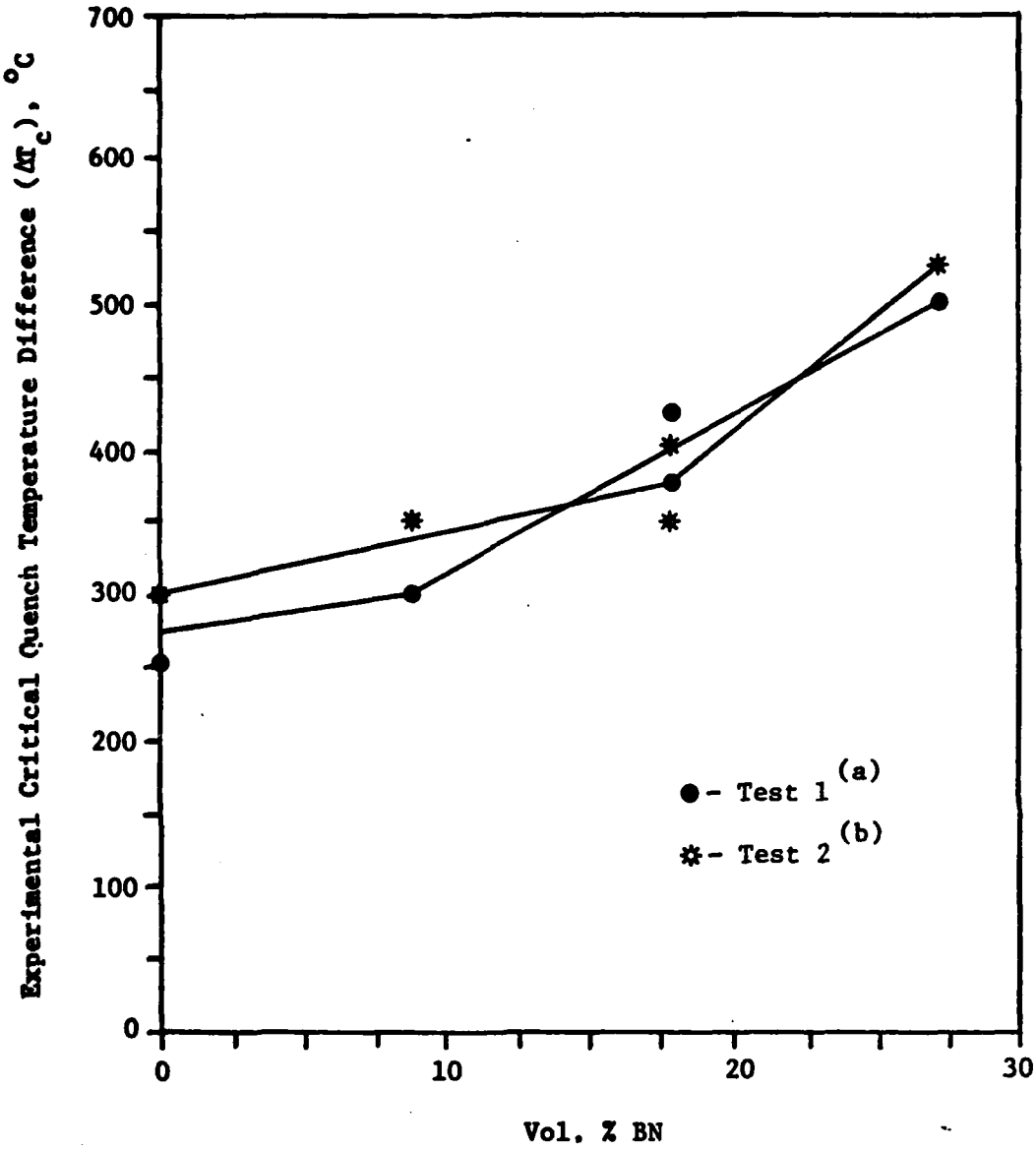

(a) Performed using optical observations.

(b) Performed at IIT Research Institute using optical observations and internal friction measurements.

Figure 16. Experimental Critical Quench Temperature Difference vs. Vol. % BN.

Table X

Thermal Shock Test Results

Composite BN Content (vol. %)	Critical Quench Temperature ΔT_c [a] Test 1 [b] (^oC)	Test 2 [c] (^oC)
0.0	303	303
0.0F	253	303
8.8	303	353
17.9	428	353
17.9P	378	403
27.2	503	528

(a) Defined as highest ΔT for survival without internal friction and/or visual evidence of damage.

(b) Performed using optical observations.

(c) Performed at IIT Research Institute using optical observations and internal friction measurements.

which was tested by standard procedures, can be expressed as

$$\sigma_b = (1.4288 \text{ cm}) \frac{P}{dh^2} \quad \text{(MPa)} \qquad (11)$$

where P is the applied load, d the specimen width, and h the specimen thickness (Fig. 17).

In general, over the composition range of 8.8 to 27.2 vol. % BN and the temperature range of 22° to 1500°C, changes in the BN content seemed to have a minimal effect on the strength of the SiC-BN composites (Table XI and Fig. 18). For the 8.8 vol. % BN specimens,

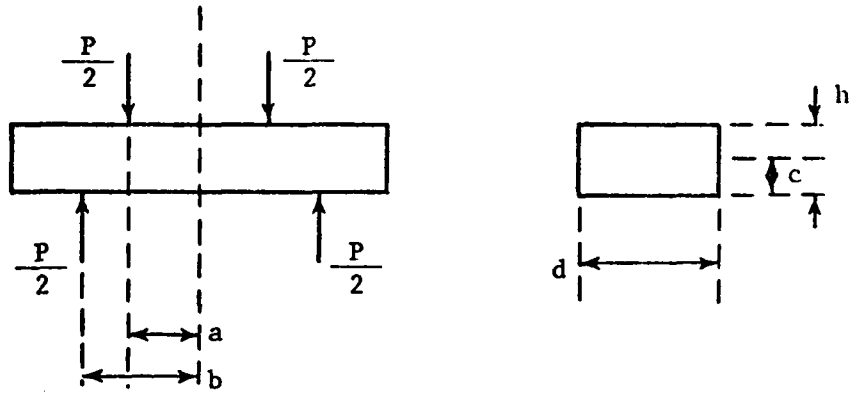

$M = \frac{P}{2}(b-a)$, the moment

$c = \frac{h}{2}$, the distance from the neutral axis to the tensile surface

$I = \frac{dh^3}{12}$, the moment of inertia

$$\sigma_b = \frac{Mc}{I}$$

$$= \frac{3P(b-a)}{dh^2}$$

for $a = \frac{3}{16}$ inch, $b = \frac{3}{8}$ inch:

$$\sigma_b = \left(\frac{9}{16} \text{ in.}\right) \frac{P}{dh^2}$$

$$\sigma_b = (1.4288 \text{ cm}) \frac{P}{dh^2}$$

Figure 17. Four-Point Bend Test.

Table XI

Bend Strengths of SiC-BN Composites[a]

Composite BN Content (vol. %)	Test Temperatures (°C) 22°	1000°	1250°	1500°
0.0	364.9	295.6	249.4	267.7
0.0F	253.4	261.3	449.6	714.5
8.8	327.4	254.0	322.8	299.0
17.9	329.0	327.1	261.3	221.3
17.9P	295.5	309.2	379.7	439.4
27.2	481.1	329.7	330.4	334.7

(a) Bend strengths in MPa.

increasing the test temperature was found to only slightly decrease the bend strength. The strength of the 17.9 and 27.2 vol. % BN specimens showed a drop in strength with increasing temperature, while the 17.9P vol. % BN specimens showed an increase in strength with temperature.

The 0 vol. % BN specimens (coarse grained) showed, also, a drop in strength as the temperature was raised, however, the 0F vol. % BN specimens showed a dramatic increase in strength with increasing temperature. The increase in strength for the 0F vol. % BN specimens (fine grained) is most likely due to the relaxation of residual stresses in the specimens that arose during cooling of the hot-pressed billet. In the 17.9P vol. % BN specimens, which were machined from the hot-pressed billet at an orientation 90° different from all of the other hot-pressed specimens, the increase in strength with temperature is probably due, in part, to the anisotropy of the SiC-BN composites. Thus,

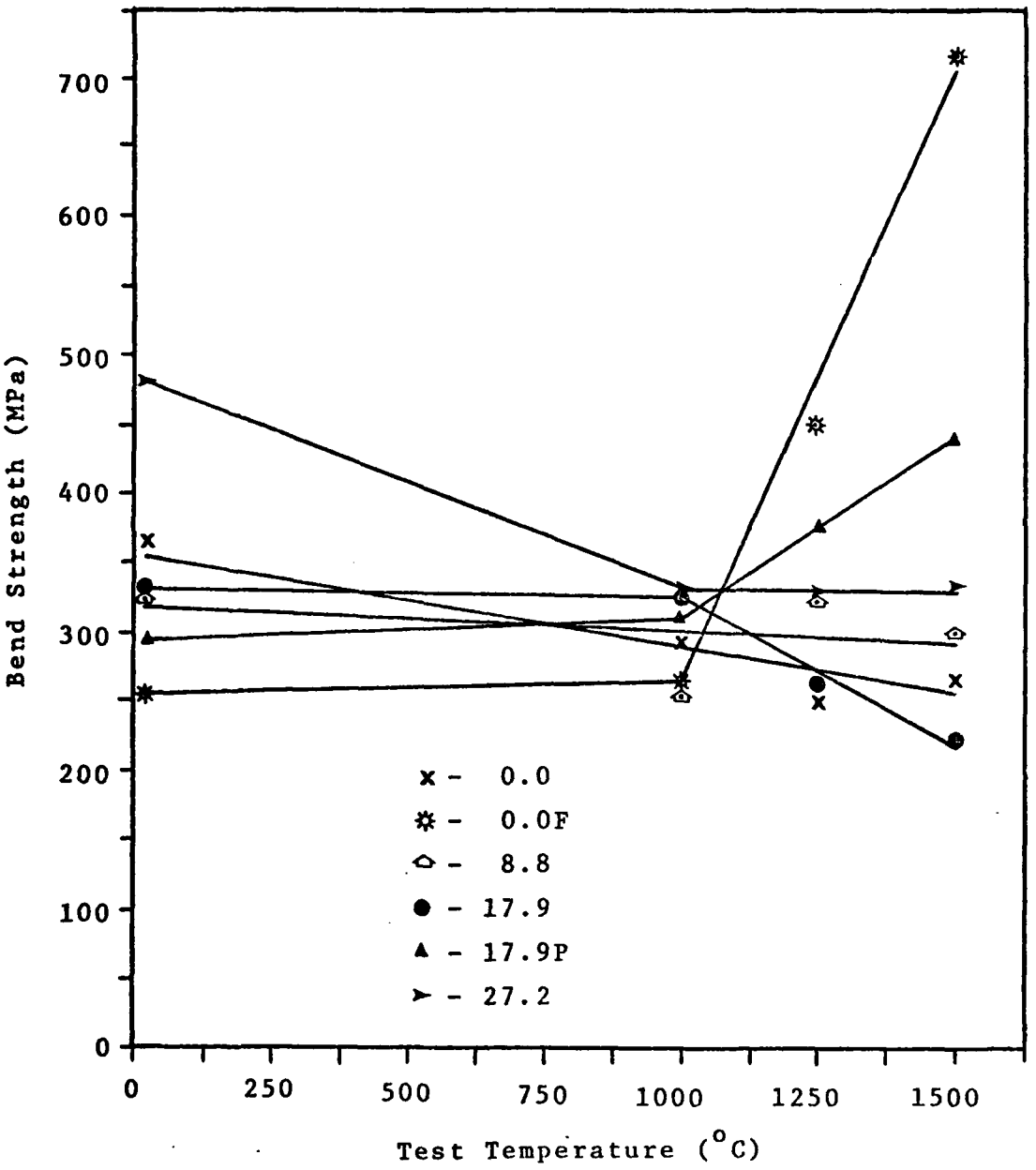

Figure 18. Bend Strength vs. Test Temperature

increasing the temperature, in general, tends to weaken the specimens, except for the cases of the fine-grained SiC specimens and the SiC-BN specimens that were machined differently.

No distinct pattern is evident for the changes in strength as a function of BN content at a constant temperature, although one would expect the strength to decrease with increasing BN content. In a study dealing with Si_3N_4-BN composites, the strength was observed to decrease with increasing BN content, although no systematic decrease with increasing BN content was observed (the authors believed this was due to the small number of samples tested) (34). Note that all of the strength results discussed above should be considered only as trends, and not as absolute variations in strength as functions of BN content and/or temperature. This is because only a small number of specimens were available for testing, two at each temperature and BN concentration.

Fracture surfaces of many of the broken composite bend bars were examined by SEM. Several of the fracture surfaces examined have been presented earlier, in Figs. 10-15 (see discussion of the microstructures of the composites). Fracture in the SiC-BN composites tends to be intragranular, thus making observations of the grain boundaries difficult. The microstructures for the coarse- and fine-grain 0 vol. % BN specimens are similar to those reported by Richerson (35) for large- and small-grained SiC samples. Although the fractures are primarily intragranular or transgranular, the BN plates are easily observed since the cracks tended to go around the plates, rather than through them. Also, when the bend bars broke, the BN plates tended to remain intact

and pull out of one side of the specimen. Thus, fracture surfaces show evidence of BN plates sticking out of the fracture "plane" or holes where BN plates had been before failure. The transgranular type failure was, also, observed by Mazdiyasni and Ruh in a study dealing with Si_3N_4-BN composites.

Fracture initiation sites, because of the rather indistinct fracture surfaces (as far as the SiC matrix is concerned), were difficult to determine. A number of possible sites were observed, though. These sites consisted of microstructural non-uniformities and surface flaws. Two possible fracture initiation sites are shown in Fig. 19. Both of these possible fracture initiation sites are examples of non-uniformities in the microstructures of the composites. The two cases shown are from the 27.2 vol. % BN specimens. The sites are both examples of areas where BN-plates grouped much closer together than usually observed. In one case (Fig. 19a), the group of BN plates was very close to the tensile surface of the bend bar. The other possible initiation site shown shows a band of non-uniform microstructure running through the bend bar (Fig. 19b). Thus, although the composite specimens had, in general, quite uniform microstructures, failure probably initiated at surface flaws and microstructural inhomogeneities (such as those shown in Fig. 19).

Influence of BN Content on the Thermal Stress Resistance Parameters of SiC

Making use of the data collected for the SiC-BN composites, values of the thermal stress resistance parameters, R, R", and R''', were calculated. The data used for the calculations included the ben

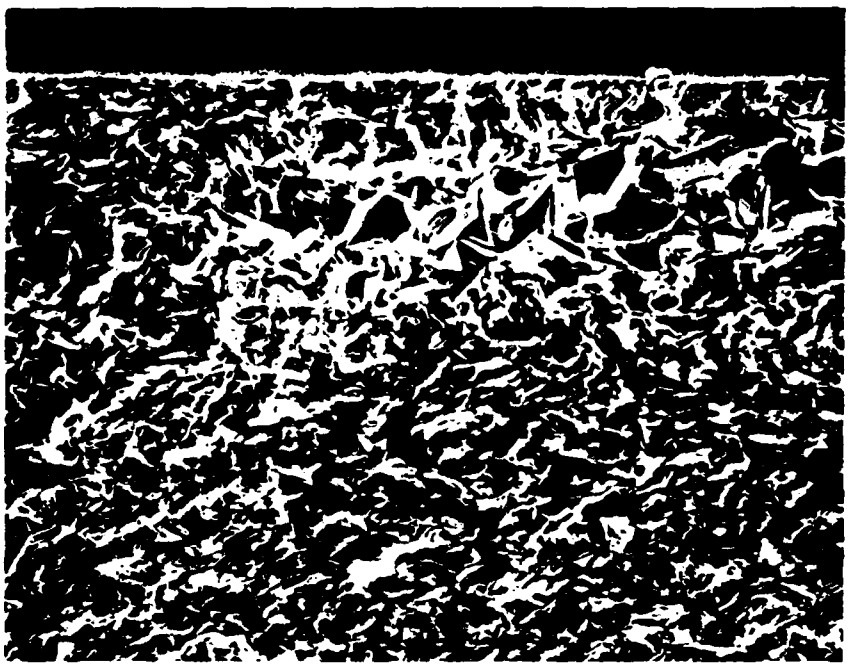

a

b

Figure 19. SEM Micrographs of Possible Fracture Initiation Sites in the 27.2 Vol. % BN Specimens ((a) and (b) 500X).

strengths, the coefficients of thermal expansion, the Young's moduli of elasticity, the Poisson's ratios, and the thermal diffusivities. All of the data used were room temperature data, except for the coefficients of thermal expansion, which were determined at 500°C for purposes of comparison with other data and since most of the specimens failed in the neighborhood of this temperature. The calculated values of R, R", and R''' are given in Table XII. Omitting the fine-grained SiC

Table XII

Thermal Stress Resistance Parameters for the SiC-BN Composites

Composite BN Content (vol. %)	$R^{(a)}$ $\{\sigma(1-\nu)\}/(\alpha E)$ (°C)	$R''^{(a)}$ $\{\sigma(1-\nu)a\}/(\alpha E)$ ($cm^{2o}C/sec.$)	R''' $E/\{\sigma^2(1-\nu)\}$ (1/MPa)
0.0	203.8	88.2	3.64
0.0F	126.9	54.9	7.85
8.8	216.6	80.0	3.60
17.9	237.5	86.0	3.34
17.9P	229.2	83.0	4.17
27.2	392.3	156.7	1.39

(a) Determined using coefficients of thermal expansion at 500°C.

specimens and the 17.9P vol. % BN specimens, the values of R increased with increasing BN content, while the values of R" showed little change up to 17.9 % boron nitride (Fig. 20). Only the 27.2 vol. % BN specimen showed a significant change, an increase, over that of the pure SiC specimen. Both of these parameters are a measure of the resistance of

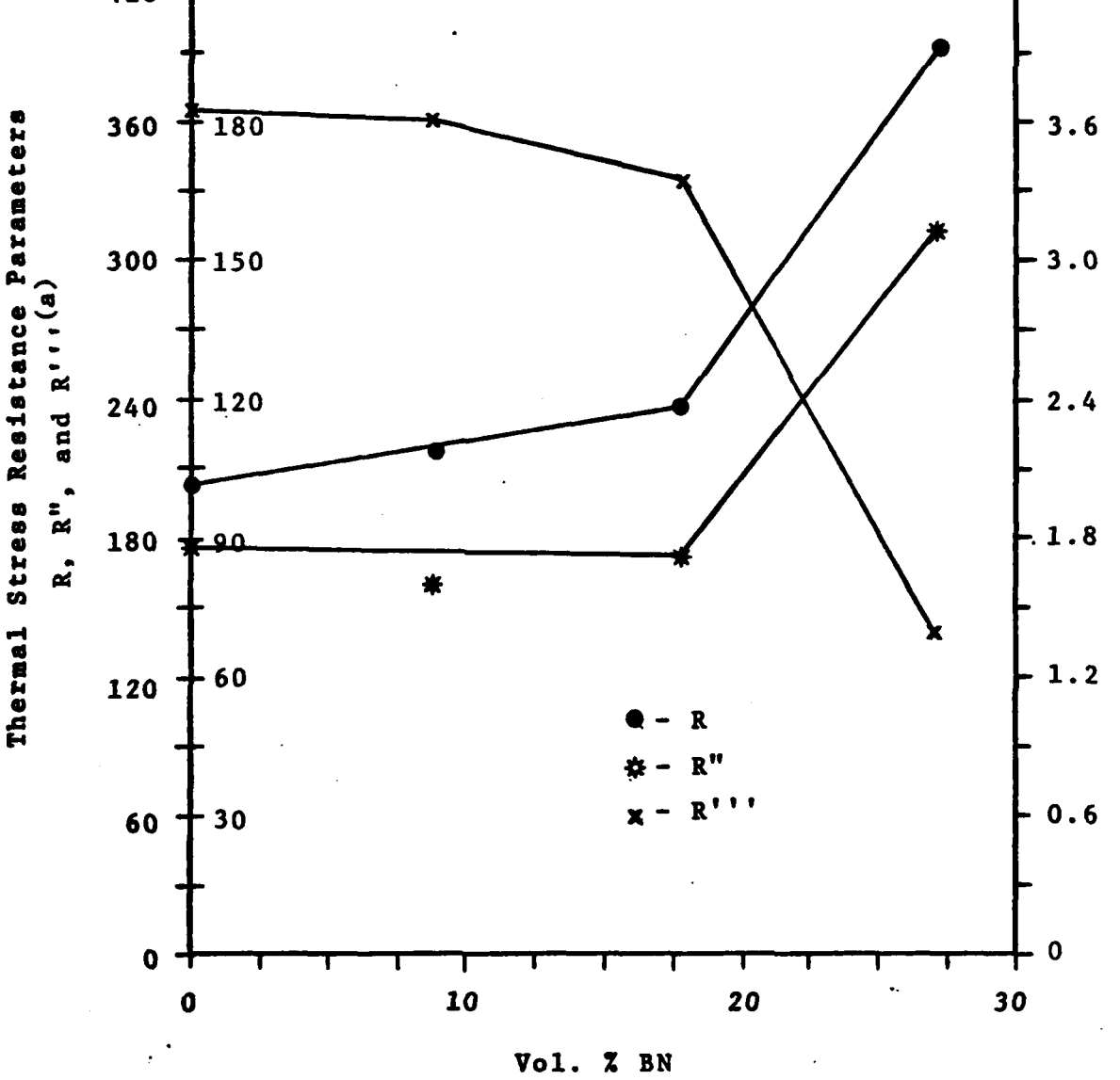

(a) Units for R, R", and R''' are (^{o}C), (cm^{2o}C/sec.), and (1/MPa), respectively.

Figure 20. Thermal Stress Resistance Parameters vs. Volume Percent BN.

a material to crack initiation. Again omitting the fine-grained SiC specimens and the 17.9P vol. % BN specimens, R''', which is a measure of the resistance of a material to crack propagation damage, was observed to decrease with increasing BN content. Therefore, increasing the BN content was observed to increase the resistance of the composites to crack initiation, while decreasing the resistance to crack propagation damage.

The fine-grained SiC specimens were found to have much lower values of R and R'' than the coarse-grained SiC specimens, but they were found to have a much larger value of R''' than the coarse-grained SiC specimens. These variations in the parameters are due primarily to the differences in bend strengths, the fine-grained SiC specimens having low bend strength at room temperature because of residual stresses. The 17.9P vol. % BN specimen, whose orientation was different from the other specimens, had values of R, R'', and R''' only slightly different from the other 17.9 vol. % BN specimen.

R, which is a measure of the resistance of a material to crack initiation, is directly related to the maximum change in temperature that can occur during quenching without causing failure (discussed earlier). Consequently, changes in the R parameter should relate directly to changes in the maximum temperature variation that a specimen can survive. Such a relationship was observed for the composites in both of the water quench tests (Table XIII). Only one of the specimens, the 17.9P vol. % BN specimen, did not obey such a relationship in one of the two sets of tests. Thus, in general, increases in the R parameter corresponded to increases in the maximum temperature difference

Table XIII

Comparison of R Parameter with Thermal Shock Test Results

Composite BN Content (vol. %)	$R^{(a)}$ $\{\sigma(1-\nu)\}/\alpha E$ (°C)	Critical Quench Temperature ΔT_c (b) (°C)	
		Test 1 (c)	Test 2 (d)
0.0	203.8	303	303
0.0F	126.9	253	303
8.8	216.6	303	353
17.9	237.5	428	353
17.9P	229.2	378	403
27.2	392.3	503	528

(a) Determined using coefficients of thermal expansion at 500°C.

(b) Defined as highest ΔT for survival without internal friction and/or visual evidence of damage.

(c) Performed using optical observations.

(d) Performed at IIT Research Institute using optical observations and internal friction measurements.

specimens could survive during quenching.

A comparison, of the results obtained in this study with the R thermal stress resistance parameters of other SiC materials, reveals that the specimens in this study have values of R similar to other SiC materials (Table XIV). Note that the 27.2 vol. % BN-SiC specimen has a value of R significantly greater than those of the other SiC materials shown in the table. Therefore, the addition of boron nitride to silicon carbide does increase the thermal stress resistance, when considering the R parameter. Similar results were obtained in a study involving additions of BN to Si_3N_4 (34). In the BN-Si_3N_4 study, thermal

stress resistance was improved by additions of boron nitride.

Table XIV

Thermal Stress Resistance Parameters for

Silicon Carbide Materials (36)

Material	R $\{\sigma(1-\nu)\}/\alpha E$ (^{o}C)
Norton NC-435 Si/SiC	244
Carborundum Sint. α-SiC	168
General Electric Sint. β-SiC	259
UKAEA/BNF Refel Si/SiC	171
UKAEA/BNF Refel Si/SiC (as processed)	140
Ceradyne 146A HP-SiC (2% Al_2O_3)	188
Ceradyne 146I HP-SiC (2% B_4C)	151
SiC-BN Composites of Present Study (0 - 27.2 vol. % BN)	127 - 392

V. Conclusions

The influence of boron nitride (BN) on the material constants and properties of silicon carbide (SiC) was examined using four different compositions, 0, 8.8, 17.9, and 27.2 volume percent boron nitride. Specifically, changes in the thermal shock resistance parameters, bend strengths, coefficients of thermal expansion, densities, and Young's moduli of elasticity were studied. Four specimens, with the above compositions, were fabricated by hot-pressing. Two other specimens were fabricated somewhat differently (by varying the processing variables), one at 0 vol. % BN and one at 17.9 vol. % BN, to observe the effects of grain size and anisotropy, respectively.

The microstructures of the composites were characterized by x-ray diffraction (XRD) analysis, density determinations, light microscopy (LM), and scanning electron microscopy (SEM). All of the hot-pressed specimens were found to be at least 97.4 % dense. XRD analysis revealed that, in all of the hot-pressed specimens, multiple polytypes of SiC were present, including β-SiC and the 2H, 4H, 6H, 15R, and 21R forms of α-SiC. In the specimens containing BN, the hexagonal α-BN form was observed. LM allowed observation of porosity and the BN particles, which were found to be aligned perpendicular to the hot-pressing direction (this alignment is due to the hot-pressing operation). SEM revealed the plate-like morphology of the BN particles in the composites. SEM also showed that one of the 0 vol. % BN-SiC specimens had a much finer grain size than the other one.

Changes in the material constants of the composite specimens, as functions of the BN content, were characterized. Both the mean

coefficients of thermal expansion and the values of the linear expansions were observed to be relatively insensitive to changes in the BN content. Changing the BN content, though, was found to have a significant effect on the Young's moduli of elasticity of the specimens. As the BN content increased, the Young's molulus decreased.

Two sets of water-quench thermal shock tests were used to characterize the thermal shock behavior of the SiC-BN composites. The results of both tests showed that increasing the BN content increased the maximum change in temperature that the composites could withstand.

The influence of BN content on the four-point bend strength of the composites was examined. Fracture surfaces were also characterized and possible fracture initiation sites were studied. In general, over the composition range of 0 to 27.2 vol. % BN and the temperature range of 22° to $1500^{\circ}C$, changes in the BN content seemed to have a minimal effect on the strength of the SiC-BN composites. However, the fine-grained 0 vol. % BN-SiC specimen showed a dramatic increase in strength with increasing temperature, probably caused by relaxation of residual stresses. No distinct pattern was evident for the changes in strength as a function of BN content at a constant temperature due to the small number of specimens considered, although one would expect the strength to decrease with increasing BN content. Fractures were primarily transgranular, although the cracks tended to go around the BN plates. Fracture initiation sites were difficult to determine because of the rather indistinct fracture surfaces, although a number of possible sites were observed. These sites consisted of surface flaws and microstructural inhomogeneities.

Using data collected for the SiC-BN composites, values of the thermal stress resistance parameters R, R", and R''' were calculated. Increasing the BN content was observed to increase the resistance of the composites to crack initiation (increase R and R"), while decreasing the resistance to crack propagation damage (decrease R'''). In general, increases in the R parameter corresponded to increases in the maximum temperature difference specimens could survive during quenching.

Anisotropy, which was studied through the use of two 17.9 vol. % BN specimens (that were machined with one having the BN plates in the test bars at an orientation 90^{o} different from those in the other specimen), had a significant effect on only the bend strengths. In one case the strength increased with temperature, while in the other case it decreased. Grain size was also found to influence the bend strengths. Of the two 0 vol. % BN-SiC specimens, the fine-grained specimen was found to have very high strength at high temperatures, while the coarse-grained specimen had much lower strength. Thus, the fine-grained specimen had low values of R and R" and a high value of R''', while the coarse-grained specimen had higher R and R" values and a lower R''' value.

Bibliography

1. W.B. Hillig, Ceramics for High Performance Applications, Vol. 2, edited by J.J. Burke, E.N. Lenve, and R.N. Katz, Brook Hill Publishing Company, Chestnut Hill, Maryland, 1978, pg. 989.

2. R.L. Mehan, G.G. Trantina, C.R. Morelock, "Properties of a Compliant Ceramic Layer," Journal of Materials Science, Vol. 16, 1981, pp. 1131-1134.

3. L.D. Bentsen, D.P.H. Hasselman, and R. Ruh, "Thermal Diffusivity of SiC-BN Composites," Basic Science Division, Fall Meeting of The American Ceramic Society, 31 October 1983, Columbus, Ohio, No. 17-B-83F.

4. D.P.H. Hasselman, P.F. Becher, and K.S. Mazdiyasni, "Analysis of the Resistance of High-E, Low-E Brittle Composites to Failure by Thermal Shock," Z. Werkstoff Tech., Vol. 11, 1980, pp. 82-92.

5. D.P.H. Hasselman and P.T.B. Shaffer, WADD-TR-60-749, Part II, 1962.

6. R.C. Rossi, Ceramics in Severe Environments, edited by W.W. Kriegel and H. Palmour III, Plenum Press, New York, 1971, pp. 123-136.

7. K.S. Mazdiyasni and R. Ruh, "High/Low Modulus Si_3N_4-BN Composite for Improved Electrical and Thermal Shock Behavior," Journal of The American Ceramic Society, Vol. 64, No. 7, July 1981, pp. 415-419.

8. D.J. Godfrey, "The Use of Ceramics in Engines," Proceedings of the British Ceramic Society, Vol. 26, July 1978, pp. 1-15.

9. W.D. Kingery, Property Measurements at High Temperatures, Factors Affecting and Methods of Measuring Material Properties at Temperatures above 1400°C (2250°F), John Wiley & Sons, Inc., New York, 1959, pp. 185-215.

10. D. Burgreen, Elements of Thermal Stress Analysis, First Edition, C.P. Press, Jamaica, New York, 1971.

11. S. Timoshenko, Theory of Elasticity, McGraw-Hill Book Co., New York, 1934.

12. L.H. Schoenlein, "Thermal Shock Resistance of an MgO-Partially Stabilized Zirconia," M.S. Thesis, Case Western Reserve University, January 1979.

13. W.D. Kingery, H.K. Bowen, and D.R. Uhlmann, Introduction to Ceramics, Second Edition, John Wiley & Sons, New York, 1976.

14. W.D. Kingery, "Factors Affecting Thermal Stress Resistance of Ceramic Materials," Journal of The American Ceramic Society, Vol. 38, No. 1, January 1955, pp. 3-15.

15. D.P.H. Hasselman, "Unified Theory of Thermal Shock Fracture Initiation and Crack Propagation in Brittle Ceramics," Journal of The American Ceramic Society, Vol. 52, No. 11, November 1969, pp. 600-604.

16. D.P.H. Hasselman, "Crack Propagation Under Constant Deformation and Thermal Stress Fracture," International Journal of Fracture Mechanics, Vol. 7, No. 2, June 1971, pp. 157-161.

17. D.P.H. Hasselman, "Thermal Stress Resistance Parameters for Brittle Refractory Ceramics: A Compendium," American Ceramic Society Bulletin, Vol. 49, No. 12, December 1970, pp. 1033-1037.

18. R.L. Coble and W.D. Kingery, "Effect of Porosity on Thermal Stress Fracture," Journal of The American Ceramic Society, Vol. 38, No. 1, January 1955, pp. 33-37.

19. D.P.H. Hasselman, "Strength Behavior of Polycrystalline Alumina Subjected to Thermal Shock," Journal of The American Ceramic Society, Vol. 53, No. 9, September 1970, pp. 490-495.

20. T.K. Gupta, "Critical Grain Size for Non-Catastrophic Failure in Al_2O_3 Subjected to Thermal Shock," Journal of The American Ceramic Society, Vol. 56, No. 7, July 1973, pp. 396-397.

21. C.Y. King and W.W. Webb, "Internal Fracture of Glass under Triaxial Tension Induced by Thermal Shock," Journal of Applied Physics, Vol. 46, No. 6, 1971, pp. 2386-2395.

22. J. Gebauer, D.A. Krohn, and D.P.H. Hasselman, "Thermal-Stress Fracture of a Thermomechanically Strengthened Alumina Silicate Ceramic," Journal of The American Ceramic Society, Vol. 55, No. 4, April 1972, pp. 198-201.

23. D.P.H. Hasselman, E.P. Chen, C.L. Ammann, J.E. Doherty, and C.C. Nessler, "Failure Prediction of the Thermal Fatigue of Silicon Nitride," Journal of The American Ceramic Society, Vol. 58, No. 11-12, Nov.-Dec. 1975, pp. 513-516.

24. W.B. Crandall and J. Ging, "Thermal Shock Analysis of Spherical Shapes," Journal of The American Ceramic Society, Vol. 38, No. 1, January 1955, pp. 44-54.

25. K. Satyamurthy, J.P. Singh, D.P.H. Hasselman, and M.P. Kamat, "Transient Thermal Stresses in Cylinders With Square Cross-Section Under Conditions of Convective Heat Transfer," Ch. X of "Thermal-Mechanical and Thermal Behavior of High-Temperature Structural Materials," Report N00014-78-C-0431 to Office of Naval Research, 1979.

26. G.H. Geiger and D.R. Poirier, Transport Phenomena in Metallurgy, Addison-Wesley Publishing Company, Reading, Massachusetts, 1973, pp. 256-263.

27. Engineering Property Data on Selected Ceramics, Volume 2, Carbides, MCIC Report/August, 1979, Metals and Ceramics Information Center, Battelle, Columbus Laboratories, 505 King Avenue, Columbus, Ohio 43201, pp. 5.2.3-1-19, 5.2.0-1.

28. P.T.B. Shaffer, "A Review of the Structure of Silicon Carbide," Acta Crystallographica, Vol. B25, 1969, pp. 477-488.

29. Engineering Property Data on Selected Ceramics, Volume 1, Nitrides, MCIC Report/March, 1976, Metals and Ceramics Information Center, Battelle, Columbus Laboratories, 505 King Avenue, Columbus, Ohio 43201, pp. 5.3.0-1, 5.3.2.2-1-9.

30. A.N. Pilyankevich and N. Claussen, "Toughening of BN by Stress-Induced Phase Transformation," Material Research Bulletin, Vol. 13, 1978, pp. 413-417.

31. "Standard Test Method for Water Absorption, Bulk Density, Apparent Porosity, and Apparent Specific Gravity of Fired Whiteware Products," ASTM Designation: C 373-72 (Reapproved 1977).

32. B.D. Cullity, Elements of X-Ray Diffraction, Second Edition, Addison-Wesley Publishing Company, Inc., 1978.

33. R. Ruh, L.D. Bentsen, and D.P.H. Hasselman, "Thermal Diffusivity Anisotropy of SiC-BN Composites," to be published.

34. K.S. Mazdiyasni and R. Ruh, "High/Low Modulus Si_3N_4-BN Composite for Improved Electrical and Thermal Shock Behavior," Journal of The American Ceramic Society, Vol. 64, No. 7, July 1981, pp. 415-419.

35. D.W. Richerson, Modern Ceramic Engineering, Properties, Processing, and Use in Design, Marcel Dekker, Inc., New York, 1982.

36. D.C. Larsen, "Property Screening and Evaluation of Ceramic Turbine Engine Materials," Technical Report AFML-TR-79-4188, Wright-Patterson Air Force Base, Ohio, October 1979.

37. C.H. Kent, "Thermal Stresses in Spheres and Cylinders Produced by Temperature Varying with Time," Journal of Applied Mechanics, Vol. 54, No. 18, 1932, pp. 185-196.

38. B. Schwartz, "Thermal Stress Failure of Pure Refractory Oxides," Journal of The American Ceramic Society, Vol. 35, No. 12, December 1952, pp. 325-333.

39. C.H. Kent, "Thermal Stresses in Thin-Walled Cylinders," Applied Mechanics (Transactions of the American Society of Mechanical Engineers), Vol. 53, No. 13, 1931, pp. 167-180.

40. W.R. Buessum, "Resistance of Ceramic Bodies to Temperature Fluctuations," Sprechsaal Fuer Keramik•Glas•Email, Silikate, Vol. 93, No. 6, 1960, pp. 137-141.

41. D.P.H. Hasselman, "Elastic Energy at Fracture and Surface Energy as Design Criteria for Thermal Shock," Journal of The American Ceramic Society, Vol. 46, No. 11, November 1963, pp. 535-540.

42. P.T.B. Shaffer and D.P.H. Hasselman, "Factors Affecting Thermal Shock Resistance of Polyphase Ceramic Bodies," Technical Documentary Report No. WADD-TR-60-749, Part II, April, 1962.

43. H.S. Carslaw and J.C. Jeager, Conduction of Heat in Solids, Second Edition, Clarendon Press, Oxford, 1959.

44. B.A. Boley and J.H. Weiner, Theory of Thermal Stresses, John Wiley, New York, 1960.

45. D.P.H. Hasselman, private communication, August 1983.

46. S. Timoshenko and J.N. Goodier, Theory of Elasticity, Second Edition, McGraw-Hill Book Company, Inc., New York, 1951, pp. 148.

Appendix A

The Thermal Stress Resistance Parameter R and the Shape Factor S for a Hollow Cylinder

An Example of Steady-State Heat Flow (17). The maximum temperature difference ($\Delta T_{max.}$) across the wall thickness of an internally heated hollow cylinder of finite length was derived by Kent (37) and applied by Coble and Kingery (18):

$$\Delta T_{max.} = \frac{\sigma_T(1-\nu)}{\alpha E}\left[\frac{2\ln(\frac{r_2}{r_1})}{\left[1-\frac{2r_1^2}{r_2^2-r_1^2}\ln(\frac{r_2}{r_1})\right]\left[1+\frac{(1+\nu^2)^{\frac{1}{2}}}{\sqrt{3}}-\nu\right]}\right] \qquad (12)$$

where the geometric term in square brackets is S and R is given by

$$R = \frac{\sigma_T(1-\nu)}{\alpha E} \qquad (3)$$

Symbols: $\Delta T_{max.}$ = maximum temperature difference

σ_T = tensile strength

ν = Poisson's ratio

α = coefficient of thermal expansion

E = Young's modulus of elasticity

r_1 = inside radius of hollow cylinder

r_2 = outside radius of hollow cylinder

To develop the above expression, thermal stress measurements were made by determining the steady-state radial temperature gradient across the

wall of a hollow cylinder necessary to cause fracture (38). The thermal stresses in the thin-walled cylinder were then analyzed (39). The maximum circumferential tensile stress (at the ends of the sample) is given by

$$\sigma_\phi = \frac{E\alpha\Delta T}{(1-\nu)} \cdot \frac{\left[1-\frac{2r_1^2}{r_2^2-r_1^2}\ln\frac{r_2}{r_1}\right]}{2\ln\frac{r_2}{r_1}} \left[1+\frac{\sqrt{1-\nu^2}}{\sqrt{3}}-\nu\right] \qquad (13)$$

where the factor $\left[1+(\sqrt{1-\nu^2}/\sqrt{3})-\nu\right]$ expresses the fractional increase of stress at the ends where free expansion may occur. The maximum temperature difference at fracture, if σ_T is the fracture stress, is given by

$$\Delta T_{max.} = \frac{\sigma_T(1-\nu)}{E\alpha} \cdot \frac{2\ln\frac{r_2}{r_1}}{\left[1-\frac{2r_1^2}{r_2^2-r_1^2}\ln\frac{r_2}{r_1}\right]\left[1+\frac{\sqrt{1-\nu^2}}{\sqrt{3}}-\nu\right]} \qquad (14)$$

$$= RS$$

where R is the thermal stress resistance parameter $\left[\sigma_T(1-\nu)/E\alpha\right]$ and S is the shape factor. Although the correction factor for end effects, $1+(\sqrt{1-\nu^2}/\sqrt{3})-\nu$, may not be exact for the wall thickness used, the relative value of thermal stress resistance calculated (R) will not change much.

Appendix B

The Thermal Stress Resistance Parameter R" and the Shape Factor S" for a Flat Plate

An Example of a Prescribed Rate of Change of Surface Temperature (17). The maximum rate of change of surface temperature until fracture for a flat plate as derived by Buessum (40):

$$(\dot{T})_{max.} = \frac{3\sigma_T(1-\nu)a}{\alpha E b^2} = \frac{\sigma_T(1-\nu)a}{\alpha E}\left[\frac{3}{b^2}\right] \qquad (15)$$

where the geometric term in square brackets is S" and R" is given by

$$R'' = \frac{\sigma_T(1-\nu)a}{\alpha E} \qquad (4)$$

Symbols: $(\dot{T})_{max.}$ = maximum rate of change of temperature

σ_T = tensile strength

ν = Poisson's ratio

a = thermal diffusivity

α = coefficient of thermal expansion

E = Young's modulus of elasticity

b = thickness of flat plate

Appendix C

The Thermal Stress Resistance Parameter R''' and the Shape Factor S''' for a Spherical Body

An Example of the Total Elastic Energy (W_T) Available for Crack Propagation (17). The total elastic energy (W_T) available for crack propagation at the instant of fracture initiation for a uniformly heated spherical body with parabolic temperature distribution, as derived by Hasselman (41):

$$W_T = \frac{4\pi b^3 \sigma_T^2 (1-\nu)}{7E} = \frac{\sigma_T^2 (1-\nu)}{E} \left[\frac{4\pi b^3}{7} \right] \tag{16}$$

where the geometric term in square brackets is the reciprocal of S''' and R''' is given by

$$R''' = \frac{E}{\sigma_T^2 (1-\nu)} \tag{5}$$

Symbols: W_T = total elastic energy

b = radius of sphere

σ_T = tensile strength

ν = Poisson's ratio

E = Young's modulus of elasticity

To develop the above expression, the material properties which govern the elastic energy at fracture and their relationship to each other can be established by considering a sphere subjected to thermal shock by heating (41,42). At the time of maximum stress, the temperature

distribution, to a good approximation, can be considered to be parabolic. The temperature rise in a sphere with arbitrary initial temperature subjected to a constant heat flux (43) is given by

$$T(r,t) = \frac{q_o b}{k}\left[\frac{3at}{b^2}+\frac{5r^2-3b^2}{10b^2}-\frac{2b}{r}\sum_{n=1}^{\infty}\frac{\sin\frac{r\beta_n}{b}e^{-\frac{at\beta_n^2}{b^2}}}{\beta_n^2\sin\beta_n}\right] \quad (17)$$

where β_n, n=1,2,3... are the roots of $\tan\beta = \beta$, r is distance from the sphere center, t is time, q_o is the initial rate of heat flux at T = 0^oK, b is the sphere radius, k is the thermal conductivity, and a is the thermal diffusivity. The non-dimensional radial and tangential thermal stresses (44) can be represented by

$$\sigma_r^* = 2\left[\frac{1}{b^3}\int_0^b Tr^2dr-\frac{1}{r^3}\int_0^r Tr^2dr\right] \quad (18)$$

and

$$\sigma_\theta^* = \frac{2}{b^3}\int_0^b Tr^2dr+\frac{1}{r^3}\int_0^r Tr^2dr-T \quad (19)$$

Using the expression for T(r,t) (42)

$$\sigma_r^* = \frac{q_o b}{5k}\left[1-\frac{r^2}{b^2}-\frac{20b^3}{r^3}\sum_{n=1}^{\infty}\frac{\sin\frac{r\beta_n}{b}-\frac{r\beta_n}{b}\cos\frac{r\beta_n}{b}}{\beta_n^4\sin\beta_n}e^{-\frac{at\beta_n^2}{b^2}}\right] \quad (20)$$

and

$$\sigma_\theta^* = \frac{q_o b}{5k}\left[1-\frac{2r^2}{b^2}-\frac{10b^3}{r^3}\sum_{n=1}^{\infty}\frac{\left[1-\frac{r^2\beta_n^2}{b^2}\right]\sin\frac{r\beta_n}{b}-\frac{r\beta_n}{b}\cos\frac{r\beta_n}{b}}{\beta_n^4\sin\beta_n}e^{-\frac{at\beta_n^2}{b^2}}\right] \quad (21)$$

The thermal stresses can be expressed in terms of tensile strength because at fracture the maximum thermal stress equals the tensile strength, assuming failure by tension. Thus, the stresses, for t approaching infinity (45), can be expressed in dimensional form as

$$\sigma_r = \frac{2\alpha E}{5(1-\nu)}\frac{qb}{k}\left[1-\frac{r^2}{b^2}\right] \quad (22)$$

and

$$\sigma_\theta = \frac{2}{5}\frac{\alpha E}{(1-\nu)}\frac{qb}{k}\left[1-\frac{2r^2}{b^2}\right] \quad (23)$$

where q is the heat flux. Since the tensile strength σ_T can be given by (42)

$$\sigma_T = \frac{2\alpha E}{5(1-\nu)}\frac{qb}{k}, \quad (24)$$

the radial and tangential stress at fracture, as a function of the tensile strength of the material, can be expressed by

$$\sigma_r = \sigma_T\left[1-\frac{r^2}{b^2}\right] \quad (25)$$

and

$$\sigma_\theta = \sigma_T\left[1-\frac{2r^2}{b^2}\right] \tag{26}$$

The elastic energy content of the sphere W is (46)

$$W = \frac{1}{2E}\int_0^b \left[\sigma_r^2+2\sigma_\theta^2-2\nu(2\sigma_r\sigma_\theta+\sigma_\theta^2)\right]4\pi r^2 dr \tag{27}$$

Substituting the expressions for σ_r and σ_θ into the elastic energy equation, the total elastic energy stored at fracture W_T is found to be

$$W_T = \frac{4\pi b^3\sigma_T^2(1-\nu)}{7E} \tag{28}$$

$$= R'''S'''$$

where R''' is the thermal stress resistance parameter $[\sigma_T^2(1-\nu)/E]$ and S''' is the shape factor. The elastic energy stored at fracture is, therefore, proportional to the sphere volume and the thermal stress resistance parameter.

Vita

Lieutenant Peter G. Valentine was born on 28 August 1957 in Dover, Delaware. He attended high school at Manchester High School in Akron, Ohio and was the valedictorian of the class of 1975. After graduating from high school, he attended Case Western Reserve University (CWRU), graduating with a Bachelor of Science degree in Metallurgy and Materials Science Engineering in May, 1979. After receiving his B.S. degree, he entered graduate school at CWRU and worked on a thesis project sponsored by the National Aeronautics and Space Administration. He was awarded a Master of Science degree in Metallurgy and Materials Science Engineering from CWRU in August, 1982. In 1981 he received a commission in the USAF through the OTS program. Upon receiving his commission, he was assigned to the Air Force Institute of Technology. He worked in the Air Force Materials Laboratory (the Processing and High Temperature Materials Branch) at Wright-Patterson AFB as an Assistant Materials Research Engineer until beginning classes in the School of Engineering in June, 1982.

Permanent Address: 5764 Eastview Drive
Clinton, Ohio 44216

UNCLASSIFIED

SECURITY CLASSIFICATION OF THIS PAGE

AD-A136891

REPORT DOCUMENTATION PAGE

1a. REPORT SECURITY CLASSIFICATION: UNCLASSIFIED	1b. RESTRICTIVE MARKINGS
2a. SECURITY CLASSIFICATION AUTHORITY	3. DISTRIBUTION/AVAILABILITY OF REPORT: Approved for public release; distribution unlimited.
2b. DECLASSIFICATION/DOWNGRADING SCHEDULE	
4. PERFORMING ORGANIZATION REPORT NUMBER(S): AFIT/GAE/AA/83D-25	5. MONITORING ORGANIZATION REPORT NUMBER(S)
6a. NAME OF PERFORMING ORGANIZATION: School of Engineering; 6b. OFFICE SYMBOL (If applicable): AFIT/ENY	7a. NAME OF MONITORING ORGANIZATION
6c. ADDRESS (City, State and ZIP Code): Air Force Institute of Technology, Wright-Patterson AFB, Ohio 45433	7b. ADDRESS (City, State and ZIP Code)
8a. NAME OF FUNDING/SPONSORING ORGANIZATION: AF Materials Laboratory; 8b. OFFICE SYMBOL (If applicable): AFWAL/MLLM	9. PROCUREMENT INSTRUMENT IDENTIFICATION NUMBER
8c. ADDRESS (City, State and ZIP Code): AFWAL/MLLM, Wright-Patterson AFB, Ohio 45433	10. SOURCE OF FUNDING NOS. — PROGRAM ELEMENT NO. / PROJECT NO. / TASK NO. / WORK UNIT NO.
11. TITLE (Include Security Classification): See Box 19	
12. PERSONAL AUTHOR(S): Peter G. Valentine, M.S., 1LT, USAF	
13a. TYPE OF REPORT: MS Thesis; 13b. TIME COVERED: FROM _____ TO _____	14. DATE OF REPORT (Yr., Mo., Day): 1983 December; 15. PAGE COUNT: 79
16. SUPPLEMENTARY NOTATION	Approved for public release: IAW AFR 190-17. 9 JAN 1984 LYNN E. WOLAVER, Dean for Research and Professional Development, Air Force Institute of Technology (ATC), Wright-Patterson AFB, OH 45433

17. COSATI CODES		
FIELD	GROUP	SUB. GR.
11	04	

18. SUBJECT TERMS (Continue on reverse if necessary and identify by block number): Silicon Carbide, Boron Nitride, Particulate Composites, Thermal Stress Resistance, Ceramics

19. ABSTRACT (Continue on reverse if necessary and identify by block number)

Title: STRENGTH AND THERMAL SHOCK RESISTANCE OF SiC-BN COMPOSITES

Thesis Chairman: Anthony N. Palazotto, Ph.D.

20. DISTRIBUTION/AVAILABILITY OF ABSTRACT: UNCLASSIFIED/UNLIMITED ☒ SAME AS RPT. ☐ DTIC USERS ☐	21. ABSTRACT SECURITY CLASSIFICATION: UNCLASSIFIED
22a. NAME OF RESPONSIBLE INDIVIDUAL: Anthony N. Palazotto, Ph.D.	22b. TELEPHONE NUMBER (Include Area Code): 513-255-3517; 22c. OFFICE SYMBOL: AFIT/ENY

DD FORM 1473, 83 APR — EDITION OF 1 JAN 73 IS OBSOLETE.

UNCLASSIFIED

SECURITY CLASSIFICATION OF THIS PAGE

The strength and thermal shock behavior of hot-pressed silicon-carbide/boron-nitride (SiC-BN) particulate composites were investigated for compositions of 0, 8.8, 17.9, and 27.2 volume percent BN. Using bend strength, Young's modulus of elasticity, density, and coefficient of thermal expansion data, the thermal stress resistance parameters R, R", and R''' were calculated and, for the R parameters, compared with experimental values for critical quench temperatures (ΔT).

Composite microstructures were characterized by x-ray diffraction (XRD) analysis, density determinations, light microscopy (LM), and scanning electron microscopy (SEM). Specimen microstructures were shown to consist of a SiC matrix with BN plates oriented perpendicular to the direction in which the load was applied during hot-pressing. Young's moduli were determined to be highly dependent on the BN content, with values decreasing with increasing vol. % BN.

In general, over the composition range of 0 to 27.2 vol. % BN and the temperature range of 22° to 1500°C, changes in the BN content seemed to have a minimal effect on the strength of the SiC-BN composites. However, a fine-grained 0 vol. % BN-SiC specimen showed a dramatic increase in strength with increasing temperature, probably caused by relaxation of residual stresses. No distinct pattern was evident for change in strength as a function of BN content at constant temperature, probably due to the small number of specimens considered, although the strength is expected to decrease with increasing BN content.

Water-quench thermal shock tests showed that increasing the BN content increased the maximum change in temperature that the composites could survive. Increasing the BN content was observed to increase the resistance of the composites to crack initiation (increase R and R"), while decreasing the resistance to crack propagation damage (decrease R'''). Grain size and anisotropy effects were also considered, with both influencing the bend strength and thermal stress resistance parameters to some extent.

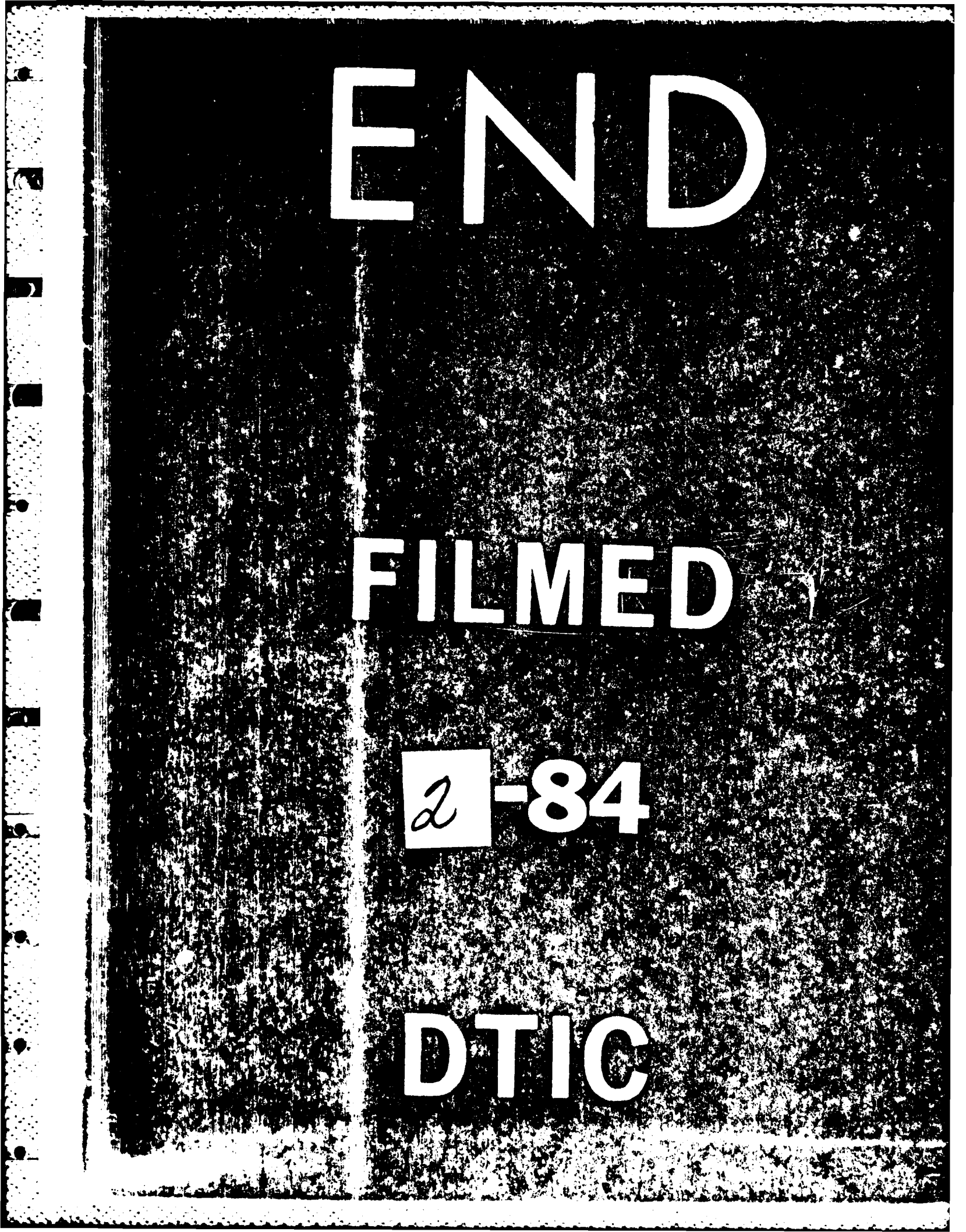
END
FILMED
2-84
DTIC